Orb weaver capture thread biomechanics and evolution

Sean D. Kelly

Thesis submitted to the faculty of the Virginia Polytechnic Institute and State University
in partial fulfillment of the requirements for the degree of

Master of Science
In
Biological Sciences

Brent D. Opell, Chair
Martha M. Muñoz
Josef C. Uyeda

May 21, 2020
Blacksburg, VA

Keywords: Bioadhesive, Biomechanics, Flagelliform fibers, Glycoprotein, Orb weaver

Orb weaver capture thread biomechanics and evolution

Sean D. Kelly

ABSTRACT

Orb weavers intercept insects using non-hardening bioadhesive droplets, supported by two flagelliform fibers. Droplets contain an adhesive glycoprotein core and aqueous layer that confers hygroscopicity. The first study investigates the durability of these droplets to cycling, or repeatedly adhering, extending, and pulling off. Droplets of four species proved resilient, cycling 40 times. Cycling, coupled with droplet humidity responsiveness, qualifies them as smart materials. However, thread adhesion is complex, relying on an integrated performance of multiple droplets and the flagelliform fibers. As insects struggle, the flagelliform fibers bow and the droplets extend, forming a suspension bridge configuration whose biomechanics sum the adhesion of droplets and dissipate the energy of struggling insects. Given this performance, the second study predicts that the material properties of both thread components have evolved in a complementary way. Comparative phylogenetics of 14 study species revealed that their elastic moduli are correlated, with glycoproteins being six times more elastic than flagelliform fibers. Spider mass affects the amount of each material, but not their properties. Since glycoprotein performance changes with humidity, we hypothesized that orb weavers generate greater adhesion at their foraging humidity. After delimiting low and high humidity species groups (eight and six species, respectively), bridge force was determined as total contributing droplet adhesion at three humidities. Only three spiders generated greater adhesion outside of their foraging humidity. The distribution of force along a suspension bridge differed from a previously reported pattern. We also characterize the sheet configuration, which generates force similar to suspension bridges.

Orb weaver capture thread biomechanics and evolution

Sean D. Kelly

GENERAL AUDIENCE ABSTRACT

In nature, adhesives are used for a variety of functions. Many animals use adhesives when climbing. Examples include toe pads of geckos, tarsal pads of ants, and tube feet of and sea urchins. Here, adhesion is repeatedly generated and released as the animal moves. However, some animals depend on permanent adhesives to anchor to surfaces. Marine mussels and barnacles, whose adult forms are sessile, use adhesives to resist the powerful action of waves and currents. Adhesion also plays a critical role in prey capture, where it prevents prey from escaping. The sticky droplets of a sundew plants and the adhesive capture threads of spider orb webs trap flies. Biologists and engineers study these bioadiehsives in search of inspiration and principles that will guide the development of new materials, including adhesives that function underwater, harden rapidly, or remaining pliable after adhering. This study investigated the material properties of capture threads spun by orb weaving spiders, which rely on non-hardening sticky droplets, supported by two protein fibers to capture insects. Inside each droplet is an adhesive core allows droplets to adhere to an insect and to extend as it struggles to escape. Surrounding this core is an aqueous layer that attracts atmospheric water, causing droplets to track changes in ambient humidity. A study of the cycling (or reusability) of four species' droplets repeatedly adhered a droplet to a surface and extending it to pull-off. These droplets were very resilient, cycling 40 times. Cycling, coupled with droplet humidity responsiveness, qualifies them as smart materials. However, prey capture is more complex, relying on the integration of multiple droplets and their supporting flagelliform fibers. As insects struggle, these fibers bow and the droplets extend, forming a suspension bridge configuration whose biomechanics sum the adhesion of droplets to resist an insect escape. The threads of 14 species were examined to test the hypothesis that material properties of both thread components have evolved in a complementary way to optimize adhesive performance. This revealed that the elasticities of the two capture thread components were correlated, with support fiber elasticity being greater. Capture threads generated the greatest adhesion at humidities during times that a spider feeds, although the distribution of this force across a suspension bridge showed different patterns among the species. The functional integration of a capture thread's components and its ability to respond to environmental humidity gives it exciting biomimicry potential.

ATTRIBUTIONS

Throughout my time at Virginia Tech, I have often felt lucky to have my advisor. Brent Opell has invested a great deal of time and energy into my future, I cannot thank him enough for that. His patience and attention to detail made this research (and my development as a scientist) possible. My time in his lab has drawn to a close, but Brent has helped me develop writing and analytical skills I will use for the rest of my career.

My committee was instrumental in the completion of my thesis. I thank Martha Muñoz for staying on my committee as a remote member at Yale University. I also thank Carlyle Brewster for his temporary service on my committee as well as Josef Uyeda for joining my committee in his place. Numerous meetings with these people have helped build a foundation for my career as an arachnologist.

I thank the American Arachnological Society for providing a place for me to hone my presenting skills. Perhaps even greater, they provided context for my work and how it fits into arachnology as a whole. They also provided me with a place to make connections with my future advisor and potential collaborators. I thank Virginia Tech Biological Sciences for creating a positive atmosphere for improving my science.

I would like to thank my parents for their open mindedness and allowing me to pursue my dreams. I also thank my four siblings, Emily, Albrey, Corey, and Ryan and their families for supporting me. Pursuing my dream has been fulfilling, but it has also taken me far from home. I thank all of my family and friends for their unconditional support and understanding.

TABLE OF CONTENTS

LIST OF FIGURES

Chapter 1:

Chapter 2:

Chapter 3:

LIST OF TABLES

Chapter 2:

Chapter 3:

LIST OF ABBREVIATONS

Chapter 2:

***LMMCs:** Low molecular mass compounds.

***RH:** Relative humidity.

L: Length of axial line as hypotenuse.

AE: Axial line extension.

$F_1/F_2/_{total:}$ Force on each axial filament and total force on droplet.

YM: Young's Modulus.

CSA_{AF}***:*** Cross sectional area of axial filament.

FL: Filament length.

****DT:*** Droplet thickness.

GV: Glycoprotein volume.

****DV:*** Droplet volume.

****GSA:*** Glycoprotein surface area

GR: Glycoprotein ratio

Chapter 3:

DW: Droplet width

DL: Droplet length

DSA: Droplet surface area

PGLS: Phylogenetic generalized least squares

*Appears in future chapters with same meaning.

Chapter 1: Introduction: Capture thread structure and biomechanics

Sean D. Kelly (Reviewed by Brent Opell)

Araneoid orb weavers are a diverse group of spiders, with the families Araneidae and Tetragnathidae consisting of over 4,000 species (World Spider Catalog, 2020). Their evolutionary success is likely due to their namesake, the ability to spin an orb web that traps flying insects with a bioadhesive (Bond and Opell, 1998). While some bioadhesives harden after secretion, as in mussels and barnacles (Dickinson et al., 2009; Waite, 2017), orb weavers employ glue droplets that remain pliable after secretion (Sahni and Dhinojwala, 2010). These viscoelastic glue droplets are situated along a pair of supporting flagelliform fibers, forming the capture spiral thread (Figure 1A) (Opell et al., 2018a). A large web surface area is critical for intercepting prey. Consequently, the distribution of adhesive as regularly spaced droplets ensures that this material is deployed in a parsimonious manner (Blackledge and Gillespie, 2002).

Orb web functionality

The capture spiral thread is the last component added to an orb web, relying on a scaffold of non-adhesive major ampullate threads for support (Foelix, 2011). Threads that form the scaffolding of the web are glued to a substrate by pyriform discs, the other bioadhesive employed by orb weavers (Wolff and Gorb, 2016). These discs form a matrix of tiny fibrils that anchor the web's frame lines to substrate (Wolff et al., 2015). Radial threads extend from the webs outer frame to its hub, forming a support for the capture thread spiral as it is deposited from periphery to the center of the web (Foelix,

2011). When an insect strikes a web the stiffer frame and radial treads absorb most of the force of impact, leaving capture threads to retain and insect until a spider can locate, run to, and subdue it (Blackledge and Eliason, 2007; Kelly et al., 2011; Sensenig et al., 2010; Sensenig et al., 2012). These threads, spun from major ampullate silk glands, are adapted to withstand impact from large and fast moving prey (Blackledge and Hayashi, 2006; Blackledge et al., 2011; Sensenig et al., 2013). Similar to the flagelliform and glycoprotein, major ampullate silk is a spidroin and belongs in a family of genes consisting of spider fibroins (Ayoub et al., 2007; Choresh et al., 2009; Collin et al., 2016; Garb, 2013; Gatesy et al., 2001; Vasanthavada et al., 2012).

Capture thread structure and adhesion biomechanics

Both components of the composite capture thread are spun from a set of three spigots located on each of a spider's paired posterior spinnerets (Coddington, 1989). As a protein fiber emerges from a flagelliform spigot, it is coated with an aqueous solution issuing from two flanking aggregate gland spigots (Opell et al., 2018a). The coated flagelliform fibers from each spinneret merge to form a cylinder, but Plateau-Rayleigh instability quickly forms the aggregate material into evenly spaced droplets (Edmonds and Vollrath, 1992; Mead-Hunter et al., 2012) (Figure 1A). Within each droplet, a glycoprotein core condenses and is responsible for the droplet's stickiness and extensibility (Opell et al., 2018a; Tillinghast et al., 1993) (Figure 1B). This core is attached to the flagelliform fibers with a granule, preventing their detachment during pull-off (Opell and Hendricks, 2010). The aggregate material that remains after glycoprotein cores is the aqueous layer (Figure 1B). This layer, which covers both the

glycoprotein and flagelliform fibers in inter-droplet thread regions, contains inorganic salts and low molecular mass compounds (LMMCs) (Townley and Tillinghast, 2013). Additional, amorphous proteins that are not visible under light microscopy also remain in the aqueous material (Amarpuri et al., 2015a).

The aqueous layer's LMMCs solvate the glycoprotein to improve its adhesion and confer droplet hygroscopicity, allowing droplet volume to track environmental humidity (Sahni et al., 2014; Townley and Tillinghast, 2013). Differences in the composition of the LMMCs confer different degrees of hygroscopicity, but other protein interactions within the droplet may play a role as well (Jain et al., 2018). Droplet extensibility increases with humidity although the magnitude of this increase differs among species (Opell and Sigler, 2011; Opell et al., 2013; Opell et al., 2018b). Higher humidities also increase a droplet's ability to flatten on a surface (Opell et al., 2013; Opell et al., 2018b). However, in some species high relative humidity results in excessive water uptake, leading to oversaturation of a droplet's glycoprotein and reduction of its viscosity, leading to cohesive failure (Amarpuri et al., 2015b; Opell et al., 2013; Sahni et al., 2011). These aspects of humidity responsiveness have created evidence that orb weavers are adapted to the humidity the forage in, a hypothesis that is supported by studies of the impact of humidity on the ability of capture threads to retain prey (Opell et al., 2017; Opell et al., 2019).

By adapting the humidity-mediated performance of their droplets to a wide range of habitats, orb weavers have been able to colonize a wide range of habitats, ranging from exposed arid habitats to humid forests (Bradley, 2013). It has also allowed orb weavers to forage at all times of the day.

Individual droplets are the smallest unit of thread adhesion, but prey capture thread adhesion occurs when multiple droplets interact with the thread's supporting flagelliform fibers (Opell and Hendricks, 2007; 2009). Moreover, successful adhesion is often the result of multiple threads contacting an insect (Chacón and Eberhard, 1980). When a capture thread is struck by an insect, its struggling causes the flagelliform fibers to bow. This bowing extends the glycoprotein of each droplet, forming a suspension bridge configuration (Figure 1C). The biomechanics of this configuration sums the adhesion of multiple droplets (Opell and Hendricks, 2009). Increased adhesion is generated by adding more droplets, although there may be diminishing returns at a certain threshold (Opell and Hendricks, 2009). In addition to the droplets, the suspension bridge configuration incorporates the work done in stretching both the droplets and the flagelliform fibers (Opell et al., 2008; Sahni and Dhinojwala, 2010). The initial modeling of the suspension bridge adhesive delivery system predicted that exterior (and more extended) droplets contribute more adhesion than interior droplets (Figure 1C) (Opell and Hendricks, 2009). However, recent work has cast doubt on the universal nature of this model (Opell and Stellwagen, 2019).

Scope of the analyses

Orb webs allow us to examine how evolution has operated on multiple scales. At a fine scale we can examine individual droplet functionality and composition. At a more comprehensive biomechanical scale, we can examine how a capture thread or an entire web functions. This study begins with a fine scale examination of single droplet biomechanics (Chapter 2) and then expands to capture thread functionality and evolution

(Chapter 3). Chapter 2 is a previously published manuscript that characterizes the ability for individual droplets to repeatedly adhere, extend, and pull-off, or cycle (Figure 1D). Using four local species of orb weavers, we compared the physical and biomechanical change in droplet performance during cycling. Droplets were largely resilient to cycling, with negligible decreases in adhesion even after 40 cycles. In fact, 40 cycles may not be close to their upper limit of reusability. This "cycling" behavior and droplet's environmental response to humidity qualifies them as smart biomaterials for the first time. The resilience of droplets allows for effective thread reattachment after a struggling insect pulls free from and then recontacts a capture thread. Chapter 3 is a broader analysis of the adhesive system, comparing suspension bridge material property evolution and biomechanics. An effective suspension bridge relies on contributions from both capture thread components as well as their integration within the system. Recent modeling reveals that synergy between the material properties of the flagelliform fibers and glycoprotein is vital suspension bridge integrity and functionality (Guo et al., 2018). The capture thread constituents are codependent in this system and because of this relationship, we predict that the material properties of both have evolved in a complementary way. This synergy hypothesis predicts that material properties will be related, increases in the elastic modulus and toughness in one will be associated with an increase in the other. However, comparative phylogenetics reveals that only elastic modulus supports this hypothesis. Knowing the variable mass of orb weavers (ranging from 7 to 800 milligrams within this study), we use the same methods to determine the impact of mass on capture thread material properties, finding that mass affects the amount of these materials, but not their properties.

The novel approach that we use to determine suspension bridge adhesion and biomechanics involved types of analyses. First, we measure thread adhesion as the sum of the force registered by the individual extended droplets in a suspension bridge and compare this summed force across three humidities. We predicted that species foraging in low humidity habitats will generate greater adhesion at lower humidities and exhibit a decrease in adhesion as humidity rises. Conversely, we predict that high humidity specialists will continue to generate greater adhesion as humidity rises. Our results largely support this hypothesis and are congruent with those of studies that support this mode of orb weaver habitat specialization. This method of droplet and suspension bridge characterization also allowed us to characterize the distribution of force along a suspension bridge. We found two main distributions of force. Half of the study species exhibit a previously modeled distribution of force, with outer droplets contributing the most adhesive force and successively inner droplets less force (Opell and Hendricks, 2009). However, the remaining species exhibited the opposite trend, with shorter interior bridge droplets generating the most adhesion. This study also characterizes an additional capture thread configuration, the sheet configuration, which occurs at high humidity when extended droplets merge. Contrary to our hypothesis, the sheet was able to generate comparable force to suspension bridges. This is explained by the observation that, as in a typical suspension bridge, the glycoprotein continues to transfer force to the bowing flagelliform fibers. Chapter 4 concludes this thesis by providing a synthesis of its findings and their significance.

Chapter 1 figure

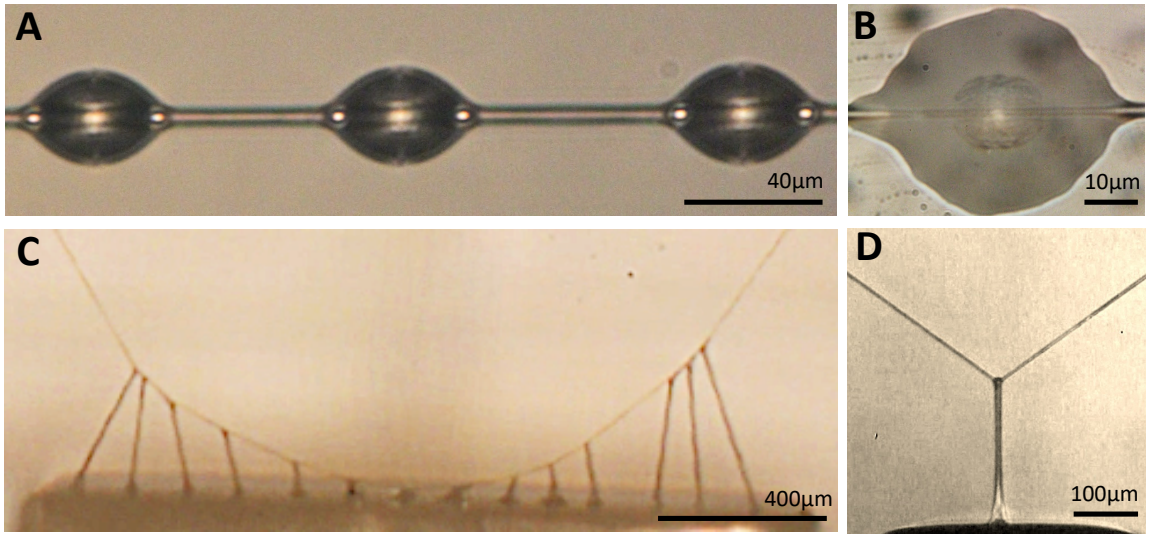

Figure 1: The various scales of an orb weaver capture thread. From the top left, 1A shows the evenly spaced ellipsoid capture thread droplets, 1B shows a droplet flattened droplet with glycoprotein core, 1C shows the suspension bridge configuration, 1D shows an individual droplet extension.

References

Amarpuri, G., Chaurasia, V., Jain, D., Blackledge, T. A. and Dhinojwala, A. (2015a). Ubiquitous distribution of salts and proteins in spider glue enhances spider silk adhesion. *Sci. Rep.* **5**,.

Amarpuri, G., Zhang, C., Diaz, C., Opell, B. D., Blackledge, T. A. and Dhinojwala, A. (2015b). Spiders Tune Glue Viscosity to Maximize Adhesion. *Am. Chem. Soc.* **9**, 11472–11478.

Ayoub, N. A., Garb, J. E., Tinghitella, R. M., Collin, M. A. and Hayashi, C. (2007). Blueprint for a High-Performance Biomaterial: Full-Length Spider Dragline Silk Genes. *PLoS One* **2**, e514.

Blackledge, T. A. and Eliason, C. M. (2007). Functionally independent components of prey capture are architecturally constrained in spider orb webs. *Biol. Lett.* **3**,.

Blackledge, T. A. and Gillespie, R. G. (2002). Estimation of capture areas in spider orb webs in relation to asymmetry. *J. Arachnol.* **30**, 70–77.

Blackledge, T. A. and Hayashi, C. Y. (2006). Silken toolkits: biomechanics of silk fibers spun by the orb web spider Argiope argentata (Fabricius 1775). *J. Exp. Biol.* **209**, 2452–2461.

Blackledge, T. A., Kuntner, M. and Agnarsson, I. (2011). *The form and function of spider orb webs. Evolution from silk to ecosystems*.

Bond, J. E. and Opell, B. D. (1998). Testing Adaptive Radiation and Key Innovation Hypothesis in Spiders. *Evolution (N. Y).* **52**, 403–414.

Bradley, R. A. (2013). *Common Spiders of North America*. Berkeley, CA: University of Califronia Press.

Chacón, P. and Eberhard, W. G. (1980). Factors affecting numbers and kinds of prey caught in artificial spider webs, with considerations of how orb webs trap prey. *Br. Arachnol. Soc.* **5**, 29–38.

Choresh, O., Bayarmagnai, B. and Lewis, R. V (2009). Spider Web Glue: Two Proteins Expressed from Opposite Strands of the Same DNA Sequence. *Biomacromolecules* **10**, 2852–2856.

Coddington, J. A. (1989). Spinneret Silk Spigot Morphology: Evidence for the Monophyly of Orbweaving Spiders, Cyrtophorinae (Araneidae), and Group Theridiidae plus Nesticidae. *J. Arachnol.* **17**, 71–95.

Collin, M. A., Ayoub, N. A. and Hayashi, C. (2016). Evidence from Multiple Species that Spider Silk Silk Glue Component ASG2 is a Spidroin. *Sci. Rep.* **6**,.

Dickinson, G. H., Vega, I. E., Wahl, K. J., Orihuela, B., Beyley, V., Rodriguez, E. N., Everett, R. K., Bonaventura, J. and Rittschof, D. (2009). Barnacle cement: a polymerization model based on evolutionary concepts. *J. Exp. Biol.* **212**, 3499–3510.

Edmonds, D. T. and Vollrath, F. (1992). The Contribution of Atmospheric Water Vapour to the Formation and Efficiency of a Spider's Capture Web. *R. Soc.* **248**, 145–148.

Foelix, R. F. (2011). *Biology of Spiders*. 3rd ed. New York, NY: Oxford Univeristy Press.

Garb, J. E. (2013). Spider Silk: An ancient biomaterial for 21st century research. In *Spider*

Research in the 21st Century (ed. Penney, D.), pp. 252–282. Siri Scientific Press, Manchester.

Gatesy, J., Hayashi, C., Motriuk, D., Woods, J. and Lewis, R. (2001). Extreme Diversity, Conservation, and Convergence of Spider Silk Fibroin Sequences. *Science (80-.).* **291**, 2603–2605.

Guo, Y., Chang, Z., Guo, H. Y., Fang, W., Li, Q., Zhao, H. P., Feng, X. Q. and Gao, H. (2018). Synergistic adhesion mechanisms of spider capture silk. *J. R. Soc. Interface* **15**,.

Jain, D., Amarpuri, G., Fitch, J., Blackledge, T. A. and Dhinojwala, A. (2018). Role of Hygroscopic Low Molecular Mass Compounds in Humidity Responsive Adhesion of Spider's Capture Silk. *Biomacromolecules* **19**, 3048–3057.

Kelly, S. P., Sensenig, A., Lorentz, K. A. and Blackledge, T. A. (2011). Damping capacity is evolutionarily conserved in the radial silk of orb-weaving spiders. *Zoology* **114**, 233–238.

Mead-Hunter, R., King, A. J. C. and Mullins, B. J. (2012). Plateau Rayleigh instability simulation. *Langmuir* **28**, 6731–6735.

Opell, B. D. and Hendricks, M. L. (2007). Adhesive recruitment by the viscous capture threads of araneoid orb-weaving spiders. *J. Exp. Biol.* **210**, 553–560.

Opell, B. D. and Hendricks, M. L. (2009). The adhesive delivery system of viscous capture threads spun by orb-weaving spiders. *J. Exp. Biol.* **212**, 3026–3034.

Opell, B. D. and Hendricks, M. L. (2010). The role of granules within viscous capture threads of orb-weaving spiders. *J. Exp. Biol.* **213**, 339–346.

Opell, B. D. and Sigler, S. E. K. M. A. (2011). Humidity affects the extensibility of an orb-weaving spider's viscous thread droplets. *J. Exp. Biol.* **214**, 2988–2993.

Opell, B. D. and Stellwagen, S. D. (2019). Properties of orb weaving spider glycoprotein glue change during Argiope trifasciata web construction. *Sci. Rep.* **9**, 1–11.

Opell, B. D., Markley, B. J., Hannum, C. D. and Hendricks, M. L. (2008). The contribution of axial fiber extensibility to the adhesion of viscous capture threads spun by orb-weaving spiders. *J. Exp. Biol.* **211**, 2243–2251.

Opell, B. D., Karinshak, S. E. and Sigler, M. A. (2013). Environmental response and adaptation of glycoprotein glue within the droplets of viscous prey capture threads from araneoid spider orb-webs. *J. Exp. Biol.* **216**, 3023–3034.

Opell, B. D., Buccella, K. E., Godwin, M. K., Rivas, M. X. and Hendricks, M. L. (2017). Humidity-mediated changes in an orb spider's glycoprotein adhesive impact prey retention time. *J. Exp. Biol.* **220**, 1313–1321.

Opell, B. D., Clouse, M. E. and Andrews, S. F. (2018a). Elastic modulus and toughness of orb spider glycoprotein glue. *PLoS One* **13**,.

Opell, B. D., Jain, D., Dhinojwala, A. and Blackledge, T. A. (2018b). Tuning orb spider glycoprotein glue performance to habitat humidity. *J. Exp. Biol.* **221**,.

Opell, B. D., Burba, C. M., Deva, P. D., Kin, M. H. Y., Rivas, M. X., Elmore, H. M. and Hendricks, M. L. (2019). Linking properties of an orb-weaving spider's capture thread glycoprotein adhesive and flagelliform fiber components to prey retention time. *Ecol. Evol.* 1–14.

Sahni, V. and Dhinojwala, A. (2010). Viscoelastic solids explain spider web stickiness.

Nat. Commun. **1**, 1–4.

Sahni, V., Blackledge, T. A. and Dhinojwala, A. (2011). Changes in the Adhesive Properties of Spider Aggregate Glue During the Evolution of Cobwebs. *Sci. Rep.* **1**, 1–8.

Sahni, V., Miyoshi, T., Chen, K., Jain, D., Blamires, S. J., Blackledge, T. A. and Dhinojwala, A. (2014). Direct Solvation of Glycoproteins by Salts in Spider Silk Glues Enhances Adhesion and Helps To Explain the Evolution of Modern Spider Orb Webs. *Biomacromolecules* **15**, 1225–1232.

Sensenig, A. T., Agnarsson, I. and Blackledge, T. A. (2010). Behavioral and biomaterial coevolution in spider orb webs. *J. Evol. Biol.* **23**, 1839–1856.

Sensenig, A. T., Lorentz, K. A. and Kelly, S. P. (2012). Spider orb webs rely on radial threads to absorb prey kinetic energy. *J. R. Soc. Interface* **9**, 1880–1892.

Sensenig, A. T., Kelly, S. P., Lorentz, K. A., Lesher, B. and Blackledge, T. A. (2013). Mechanical performance of spider orb webs is tuned for high-speed prey. *J. Exp. Biol.* **216**, 3388–3394.

Tillinghast, E. K., Townley, M. A., Wight, T. N., Uhlenbruck, G. and Janssen, E. (1993). The adhesive glycoprotein of the orb of Argiope aurantia (Araneae, Araneidae). *Mater. Res. Soc. Symp. Proc.* **259**, 154–165.

Townley, M. A. and Tillinghast, E. K. (2013). *Aggregate Silk Gland Secretions of Araneoid Spiders*. (ed. Nentwig, W.) Springer-Verlag Berlin Heidelberg.

Vasanthavada, K., Hu, X., Tuton-Blasingame, T., Hsia, Y., Sampath, S., Pacheco, R., Freeark, J., Falick, A. M., Tang, S., Fong, J., et al. (2012). Spider glue proteins have distinct architectures compared with traditional spidroin family members. *J. Biol. Chem.* **287**, 35985–35999.

Waite, H. J. (2017). Mussel adhesion - essential footwork. *J. Exp. Biol.* **220**, 517–530.

Wolff, J. O. and Gorb, S. N. (2016). *Attachment Structures and Adhesive Secretions in Arachnids*. New York, NY: Springer.

Wolff, J. O., Grawe, I., Wirth, M., Karstedt, A. and Gorba, S. N. (2015). Spider's super-glue: thread anchors are composite adhesives with synergistic hierarchical organization. *Soft Matter* **11**, 2394–2403.

World Spider Catalog (2020).

Chapter 2: Orb weaver glycoprotein is a smart biological material, capable of repeated adhesion cycles

Sean D. Kelly, Brent D. Opell, & Lindsey L. Owens

Published in The Science of Nature *Kelly, S.D., Opell, B.D. & Owens, L.L. Orb weaver glycoprotein is a smart biological material, capable of repeated adhesion cycles. Sci Nat* ***106,*** *10 (2019).* https://doi.org/10.1007/s00114-019-1607-z

ABSTRACT

Orb weavers produce webs that trap prey using a capture spiral formed of regularly spaced glue droplets supported by protein fibers. Each droplet consists of an outer aqueous layer and an adhesive, viscoelastic glycoprotein core. Organic and inorganic compounds in the aqueous layer make droplets hygroscopic and cause droplet features to change with environmental humidity. When droplets contact a surface, they adhere and extend as an insect struggles. Thus, a droplet's extensibility is as important for prey capture as its adhesion. Cursory observations show that droplets can adhere, extend, and pull-off from a surface several times, a process called cycling. Our study cycled individual droplets of four species: *Argiope aurantia, Neoscona crucifera, Verrucosa arenata,* and *Larinioides cornutus*. Droplets were subjected to 40 cycles at two humidities to determine how humidity affected droplet performance. We hypothesized that droplets would continue to perform, but that performance would decrease. Droplet performance was characterized by filament length and force on droplets at pull-off, aqueous volume, and glycoprotein volume. As hypothesized, cycling decreased performance, notably extensibility and aqueous volume. However, humidity did not impact the response to cycling. In a natural context, droplets are not subjected to extensive cycling, but reusability is advantageous for orb weaving spiders. Moreover, the ability to cycle, combined with their environmental responsiveness, allows us to characterize orb weaver droplets as smart materials for the first time.

Key Words: glycoprotein, orb weaver, smart material, adhesion, viscous capture droplet, spider web

Introduction:

Bioadhesives are natural materials that adhere surfaces together and are used by many organisms (Palacio and Bhushan 2012). For example, mussels and barnacles attach to substrates with bioadhesives (Naldrett 1993; Dickinson et al. 2009; Kamino 2010; Waite 2017). Caddis fly larvae and some polychaete annelids use an adhesive to construct a protective tube from sand and shell fragments, and many insects use adhesives to attach their eggs (Mackay and Wiggins 1979; Jensen and Morse 1988; Li et al. 2008). Like most commercial adhesives, these bioadhesives harden after they are applied. In contrast, bioadhesives that are used by sundews, onychophorans, and orb-weaving spiders remain pliable after they are produced, ensuring that they spread to establish adhesive contact with insects they capture (Concha et al. 2015; Huang et al. 2015). An orb-weaving spider's adhesive takes the form of regularly spaced viscoelastic glue droplets, which form the capture spiral thread of their web (Figure 1a). Each droplet consists of a glycoprotein core surrounded by an aqueous outer layer (Figure 1b). Together, the droplets along a thread retain an intercepted prey long enough for the spider to locate and subdue it (Blackledge and Eliason 2007). When a series of droplets contact an insect, they extend as the insect struggles, thus combining their adhesive forces and dissipating the energy of the struggling prey (Opell and Hendricks 2007; Sensenig et al. 2013).

Because orb weaver glycoprotein remains pliable, we hypothesize that it functions as a smart material, one that possesses "the ability to change their physical properties in a specific manner in response to specific stimulus input. The stimuli could be pressure, temperature, electric and magnetic fields, chemicals, hydrostatic pressure or nuclear radiation." (Kamila 2013). Additionally, smart materials must exhibit a reversible behavior or "cycling" in order to be classified as such (Talbot 2003; Smith 2006; Hoogenboom 2014). In the case of our system, orb weaver glue droplets respond to cycling by changing their volume and extensibility as relative humidity changes (Opell et al. 2018a, b). However, the other component of a smart material, cycling, has not been well documented for this bioadhesive. When glycoprotein within droplets that had been flattened on a microscope slide was extended with the tip of a glass probe, the glycoprotein continued to extend for 13 cycles (Sahni and Dhinojwala 2010). However, the ability of native, suspended droplets to cycle through multiple contact, extension, and

pull-off cycles has not been documented. We test our hypothesis by repeatedly adhering individual glue droplets of four orb-weaving species at two different humidities. These individual droplets were adhered to a probe 40 times, and droplet performance was characterized throughout adhesion cycles. If cycling is documented, then we can classify orb weaver droplets as smart materials, enhancing their potential for biomimicking studies.

Orb webs are constructed from four types of silk, each secreted by a different gland and exhibiting unique properties (Blackledge and Hayashi 2006; Foelix 2011). The major ampullate glands, situated on the anterior lateral spinnerets, secrete both the stiff frame and radial threads of an orb web (Coddington 1989). Frame threads are attached to surfaces with shock-absorbing pyriform disks and are secreted from a cluster of silk glands of the same name, also located on the anterior spinnerets (Jain et al. 2014; Wolff et al. 2015). Radial threads support the capture spiral and absorb kinetic energy from flying prey (Sensenig et al. 2012). The capture spiral is the product of two types of silk glands, both located on the posterior spinnerets—flagelliform glands, which produce a pair of axial lines, and aggregate glands, which simultaneously cover the axial line in an aqueous glue solution (Edmonds and Vollrath 1992; Opell and Hendricks 2007; Opell et al. 2018b, a). Aggregate glands are unique to the superfamily Araneoidea and are considered to be a key innovation that contributed to the group's evolutionary success (Coddington 1989; Bond and Opell 1998; Blackledge et al. 2009; Townley and Tillinghast 2013). Capture thread is a self-organizing material, whose aqueous layer initially forms a cylinder around the axial threads and then is reconfigured by Plateau–Rayleigh instability into evenly spaced ellipsoid droplets along the supporting axial fibers (Vollrath and Tillinghast 1991; Edmonds and Vollrath 1992; Mead-Hunter et al. 2012). These glue droplets not only trap insects but also play a key role in maintaining the mechanical robustness of the web, with their ability to spool and pack the axial fibers internally, preserving the tension of the capture thread (Elettro et al. 2016). After a glycoprotein core forms within each droplet, the remaining aggregate gland material remains as an aqueous layer, which covers both the glycoprotein and axial fibers. This layer influences droplet size, as well as glycoprotein adhesion (Vollrath and Tillinghast 1991; Sahni et al. 2014). Low molecular mass compounds (LMMCs) within the aqueous

layer, such as choline chloride and N-acetyltaurine, confer hygroscopicity to droplets, causing their volume and performance to change over the course of a day with ambient humidity (Townley et al. 1991; Edmonds and Vollrath 1992). LMMCs also solvate the glycoprotein and improve adhesion, while maintaining the glycoprotein structure (Sahni et al. 2014; Amarpuri et al. 2015a, b). This water plasticizes the capture spiral thread, allowing for greater extension, which is beneficial for prey capture (Vollrath and Edmonds 1989; Blackledge and Hayashi 2006). Natural selection has tuned droplet hygroscopicity by altering the composition of a thread's LMMCs, conferring greater hygroscopicity to threads spun by orb weaving species that are found in exposed, lower humidity habitats than to the threads of species that occupy humid forest habitats (Opell et al. 2013; Amarpuri et al. 2015a, b).

Although the aqueous layer influences adhesion, the glycoprotein is directly responsible for it, contributing an order of magnitude more adhesion than the capillary force generated by the aqueous layer (Tillinghast et al. 1993; Sahni and Dhinojwala 2010). At the center of each glycoprotein core, there is a denser region termed a "granule" that appears responsible for anchoring the droplet to the axial lines, minimizing sliding as droplets are extended (Opell and Hendricks 2010). Despite being highly pliable, the glycoprotein is a spidroin (a class of spider scleroproteins) similar to other orb web components (Gatesy et al. 2001; Ayoub et al. 2007; Garb et al. 2010). To date, only one glycoprotein has been characterized—AgSp1 (aggregate spidroin 1) also known as ASG2 (Choresh et al. 2009; Collin et al. 2016). Although glycoprotein is visible only in a droplet's core, proteins are also distributed ubiquitously throughout the aqueous layer (Amarpuri et al. 2015a, b).

When droplets adhere to an insect, the glycoprotein core in each droplet extends, forming an aqueous layer-covered filament that contributes adhesion responsible for holding the insect in place as it attempts to pull free from the web (Figure 1c). Humidity significantly impacts maximum droplet filament length by altering glycoprotein viscosity (Opell and Sigler 2011; Sahni et al. 2011; Opell et al. 2013; Amarpuri et al. 2015a, b). As mentioned, natural selection has tuned droplet hygroscopicity by altering the LMMC composition, optimizing adhesion in different habitats. This system offers potential for chemists seeking to develop environmentally responsive adhesives. Smart materials are

of particular interest for bioinspired development because these materials combine both environmental responsiveness and cycling, the ability to repeatedly perform a task or exhibit a behavior. Examples of such materials include a grass seed's awn, which opens and closes in response to humidity to actively propel the seed into the soil (Elbaum et al. 2007) (Figure 2).

It is clear that viscous capture droplets are environmentally responsive, although their cycling has not been documented. In nature, a struggling insect is likely to pull free from a thread's glue droplets and, then, re-adhere to them. Thus, there is reason to believe that our cursory observations of droplets re-adhering and extending several times after pull-off are integral characteristic of viscous capture thread performance. In our experimental system, one droplet cycle consists of adhesion to a surface, extension, and pull-off. The objective of this study was to test the following hypotheses: (1) orb weaver glycoprotein is capable of cycling many times with only moderate loss of performance and (2) humidity affects cycling durability, with a more pronounced decrease at low humidity. We characterized droplet cycling by capturing videos of extending droplets and still images of suspended droplets before and after each of 40 cycles. From these, we determined the following: (1) droplet filament length at pull-off, (2) force on a droplet at pull-off, (3) droplet volume and symmetry, and (4) glycoprotein surface area. We tested these hypotheses by characterizing the cycling of four orb-weaving species' droplets. Each species' droplets were cycled at two humidities, representing the upper and lower ranges of humidity encountered during its foraging period.

Changes in glycoprotein performance during cycling would be expressed as a reduction in maximum droplet extension and by less force on an extended droplet at pull-off, as gauged by the deflection of the droplets' support line. Repeated cycling may also affect how LMMCs bind to glycoproteins, an interaction that is crucial for maintaining glycoprotein structure (Amarpuri et al. 2015a, b). This could also indirectly impact glycoprotein viscosity by adding or subtracting LMMCs from the aqueous layer, thereby altering droplet hygroscopicity and volume (Amarpuri et al. 2015a, b).

Materials and methods:

Collecting and preparing threads

We collected orb web samples from 9 to 11 mature females of the following species: *Argiope aurantia* Lucas 1833, *Verrucosa arenata* (Walckenaer 1842), *Larinioides cornutus* (Clerck 1757), and *Neoscona crucifera* (Lucas 1839). We collected these samples from August 1st to September 29th, 2017 near Blacksburg, Virginia. *Argiope aurantia* build their webs in exposed weedy habitats before dawn for use throughout the day (Enders 1977). Argiope aurantia droplets are very hygroscopic, which is an advantage when relative humidity drops in late morning and afternoon (Opell et al. 2013). *Verrucosa arenata* is diurnal like *A. aurantia*, but its shaded forest habitat exposes its webs to higher humidities than *A. aurantia* (Gaddy 1987; Opell and Hendricks 2009). *Larinioides cornutus* and *N. crucifera* are both nocturnal but vary in their microhabitat. *Larinioides cornutus* spin their webs on man-made structures or vegetation near water, whereas *N. crucifera* spin their webs along the forest edge at dusk (Adams 2000; Bradley 2013). We collected all web samples shortly after their construction to ensure that droplets were not contaminated by dust or pollen.

A 15 × 52-cm rectangular aluminum frame with double- sided 3M tape (3M #9086K29550360) on one face was pressed against capture threads in the outer part of a web, securing the contacting threads and separating the sample from the web. After collection, we placed the frame in a closed container for transport to the laboratory, where they were stored at 50–55% relative humidity (RH). We marked the web's position with flagging tape to prevent resampling.

To ensure that we extended only fresh droplets, we completed all extension trials within 17 h after thread collection. We collected individual threads using a pair of forceps with double-sided carbon tape (Cat #77816, Electron Microscope Sciences, Hatfield, PA, USA) wrapped around the tips. These forceps were blocked open to accommodate the supports on a microscope slide sampler where threads were placed. After the forceps tips contacted a thread, we used a hot probe to sever the thread from the web sample. These procedures ensured that threads placed on sampler remained at their native tensions. The microscope slide sampler consisted of four U-shaped brass supports, spaced at 4.8 mm intervals with their upper surfaces covered with carbon tape (Opell and Sigler 2011).

Extending droplets

After collecting the thread samples, we isolated a droplet at the center of the 4.8 mm thread span. To do this, we first sharpened the tip of a small wooden applicator stick so that a few fibers extended and saturated the tip in distilled water. Using this fine point, we slid away the droplets on either side of the focal droplet.

Samplers were placed in a glass-covered observation chamber that rested on the mechanical stage of a Mitutoyo inspection microscope. The chamber maintained a temperature of 23 °C and permitted control of humidity during trials (Opell et al. 2013). We extended individual droplets from each species at two relative humidities separated by 18% RH, chosen to represent divergent, but representative values from each species' habitat. The values were based on measurements of these species' droplet extensions (Opell et al. 2013). We selected lower values (37% and 55% RH) for *A. aurantia* based on its exposed habitat and highly hygroscopic droplets (Enders 1977; Carrel 2008; Opell et al. 2013). We selected higher values (55% and 72% RH) for the remaining species based on the higher humidity of their habitats and the lower hygroscopicity of their droplets (Gaddy 1987; Adams 2000; Bradley 2013).

Before extending a droplet, we cleaned the 413-μm-wide polished tip of a steel probe with 95% ethanol on a Kimwipe®. We, then, inserted the probe through an adjustable plate on the side of the observation chamber. After we aligned the probe with the droplet, the plate was secured, and the protruding probe was, then, locked in a device that prevented its movement. The observation chamber holding the thread sample was advanced using the microscope stage's X-axis manipulator, bringing the thread into contact with the probe tip and, then, advanced an additional 250 μm to ensure droplet adhesion. The droplet was, then, immediately extended at 69.5 μm s^{-1} by engaging a stepping motor that activated the microscope X-axis manipulator, while a video recorded the droplet's extension at 60 frames per second.

Each droplet extension cycle consisted of droplet adhesion, droplet extension, and droplet pull-off. Thus, we characterized a droplet's ability to adhere and perform by measuring the following: the length of its extending filament, the force on the droplet at pull-off, and the ability of the droplet to remain attached to the axial line. We extended each droplet 40 times, except in a few cases where the droplet pulled free of the thread and remained on the probe's tip. We designated the 1st, 2nd, 4th, 8th, 16th, 24th, 32nd,

and 40th extensions as focal extensions, recording videos of these extensions and capturing an image of the droplet before and after each of these extensions. This was done to emphasize earlier extensions, where we presumed that most changes in droplet performance would occur.

Each cycling sequence was conducted as a series, with the time between cycles determined by the short period needed to advance and contact the probe and start the video recording. As the same operator (SDK) performed all extensions, this interval was uniform throughout the study. Thus, droplet recovery period was very similar between cycles and among species. Although, inter-specific differences in glycoprotein viscosity would affect the rate of recovery, we confine our analysis to comparing only intra-specific effects of cycling.

Characterizing droplet volume and symmetry

Droplet volume was determined from images taken before cycling began and after the 40th extension. We used Onde Rulers v1.13.1 screen caliper (Ondesoft Computing, Inc., Beijing, China) to measure droplet length and width (*DL* and *DW*, respectively) of suspended droplets. We also measured another droplet, termed a reference droplet, taken from the same web for use in comparison of the glycoprotein volume, as described subsequently. Droplet volume (*DV*) was computed using the formula presented in (Liao et al. 2015) and shown as follows:

$$DV = \frac{2\pi\ (DW)^2\ x\ DL}{15} \tag{1}$$

This formula assumes that droplets are a symmetrical ellipsoid. While this assumption worked for fresh droplets, excessive cycling often altered the shape of droplets, making them laterally asymmetrical (Figure 3b). For these droplets, we relied on the penultimate formula reported in the derivation series that produced the formula shown previously.

$$DV = \frac{16\,\pi\,\left(\frac{DW}{2}\right) x\,(\frac{DW}{2})\,x\,(\frac{DL}{2})}{15} \quad (2)$$

This formula allowed us to distinguish the asymmetrical protrusion of a droplet on either side of the axial line. However, in more complex instances of asymmetry, we modeled droplet volume as the sum of an ellipse, cones, and cylinders (Figure 4a, b). Instead of squaring droplet width (DW), we measured each side independently, thus accounting for droplet asymmetry. We characterized the symmetry of droplets throughout cycling by measuring the width of the droplet on each side of its flagelliform fiber midline and dividing the shorter of the two by the longer. Thus, a perfectly symmetrical droplet would have a symmetry index of 1 and asymmetrical droplets' smaller values (Table 1).

The aqueous material that covers each droplet's glycoprotein core also continues into inter-droplet regions, where it covers the flagelliform fibers. Therefore, it is possible that this material may flow from the droplet into the inter-droplet regions with cycling. To determine if this occurred, we measured the diameter of the inter-droplet region approximately one droplet diameter away from the edge of a droplet before cycling and after 40 extension cycles. This allowed us to test the hypothesis that repeated cycling drew aqueous material from a droplet and explained any difference in droplet that we might detect between fresh and cycled droplets (Table 2).

Characterizing visible glycoprotein using reference droplets

After the 40th extension, a droplet was flattened to reveal its glycoprotein core (Figure 3c, d). We accomplished this by using a magnetically tipped device to drop a 22-mm-diameter cover- slip on the threads. Once dropped, we pressed the coverslip against the sampler supports using the steel probe to ensure uniform droplet flattening. We also flattened an unextended reference droplet from the same individual's web, to allow a comparison of the effect of droplet cycling on glycoprotein volume and a droplet's glycoprotein volume to aqueous layer volume ratio.

We determined glycoprotein volume (*GV*) from droplet thickness (*DT*) and glycoprotein surface area (*GSA*). First, we used droplet volume (DV) and flattened

droplet surface area (*DSA*) to obtain droplet thickness. The product of *DT* and *GSA* gave us *GV*:

$$DT = \frac{DV}{DSA} \tag{3}$$

$$GV = DT\ x\ GSA \tag{4}$$

Glycoprotein ratio (GR) was determined from glycoprotein volume and droplet volume (GV and DV, respectively), using the following formula:

$$GR = GV/DV \tag{5}$$

Characterizing filament length, force on a droplet at pull-off, and estimated work of droplet extension

The length of an extending droplet filament at pull-off was measured using Onde Rulers v1.13.1 screen caliper (Ondesoft Computing, Inc., Beijing, China) (Figure 1c). Using the method from (Opell et al. 2018a, b), we computed the force on drop- lets at pull-off in four steps (Figure 2). This approach uses the extension of the paired axial support lines on each side of a droplet with the reported diameters and Young's modulus of these lines (Sensenig et al. 2010) to determine the force on each side of the deflected support line. These force vectors are, then, resolved to determine the force on an extended droplet filament.

Step 1: Length of the axial line on each side of the extended droplet, computed as a hypotenuse of the right triangle (*L*) with an opposite side of 2400 μm and an angle between the hypotenuse and adjacent sides of a right triangle, which is equal to one half of the support line deflection angle (Θ).

$$L = \frac{2400\mu\text{m}}{\sin\frac{\Theta}{2}} \tag{6}$$

Step 2: Axial line extension (AE) ratio.

$$AE = \frac{(\mathrm{L} - 2400\mu\mathrm{m})}{2400\mu\mathrm{m}} \tag{7}$$

Step 3: Force on axial line (F_1) as a product of Young's modulus (YM), the sum of the two axial line's cross-sectional areas (CSA_{AF}), and axial line extension (AE). *A. aurantia*, *V. arenata*, *L. cornutus*, and *N. crucifera* YM = 0.009, 0.098, 0.011, and 0.010 GPa, respectively, and each axial line diameter = 4.8, 1.5, 2.6, and 3.0 µm, respectively.

$$F_1 = F_2 = YM \ \mathrm{x} \ CSA_{AF} \ \mathrm{x} \ AE \tag{8}$$

Step 4: Force on extended droplet filament (F_{total}) as the resolved force vectors of the two sides of the support line (F_1), which are equal, using the deflection angle of the support line (Θ).

$$F_{total} = 2 \ \mathrm{x} \ F_1 \ \mathrm{x} \ \sin(90° - \left(\frac{\Theta}{2}\right)) \tag{9}$$

We estimated the work in joules required to extend droplets to pull-off as the product of the amount of glycoprotein (glycoprotein volume = *GV*), its viscosity (droplet thickness = glycoprotein thickness = *DT*), and the length of its extension (filament length = *FL*), using the following formula.

$$Estimated\ Work\ in\ joules = FL\ x\ DT\ x\ GV \tag{10}$$

Assessing residue on the probe tip after droplet cycling

To determine if repeated cycling left LMMCs or glycoprotein residues on the probe's steel surface, we cleaned a small broken piece of a razor blade with 100% ethanol and contacted it 40 times at 50% RH with an *L. cornutus* droplet. This sample was attached to a scanning electron microscope stub and stored in a desiccator for approximately two weeks, sputter coated with 3 nm of iridium before examination with a LEO (Zeiss) 1550 FESEM (field emission scanning electron microscopy) at the

Nanoscale Characterization and Fabrication Laboratory (NCFL) at Virginia Tech, in an attempt to identify compounds in any residue present on the sample.

Analysis

Data were analyzed using SAS JMP (SAS Institute Inc. 1989– 2007). We evaluated parameter normality using a Shapiro– Wilk test, considering values with $P \geq 0.05$ to be normally distributed. Parametric and nonparametric tests with $P \leq 0.05$ were considered significant. Matched pairs were used for most before–after cycling comparisons.

Four trials were excluded because their droplets pulled off of the axial thread and adhered to the probe. This occurred in one *N. crucifera* individual at 72% RH, one *A. aurantia* individual at 55% RH, and two *V. arenata* individuals at 72% RH. For these trials, we included only extensions prior to droplet detachment. Droplets that extended fewer than 40 times were included, although this only occurred in two *N. crucifera* individuals and a single *V. arenata*. One *N. crucifera* individual whose droplet divided into two smaller droplets was excluded from further extensions at low humidity.

Results:

Droplet symmetry, droplet volume, and glycoprotein volumes

Droplet symmetry decreased after cycling in all treatments (Table 1). The initial volume of the extended droplets did not differ from that of the reference droplets (Table 3). However, droplet volume decreased in all treatments after cycling except *V. arenata* and *N. crucifera* at low humidity (Table 1, Tables 5-8). In contrast, glycoprotein volume either remained unchanged or increased (only in *A. aurantia* at 55% humidity) (Table 4). Therefore, as confirmed by the ratio of glycoprotein volume to total droplet volume (Table 4), the decrease in droplet volume resulting from cycling is explained by the loss of aqueous material. The diameters of inter-droplet diameters were not affected by cycling ($P = 0.9096$, 0.6741, 0.6029, and 0.2850 for *A. aurantia*, *V. arenata*, *L. cornutus*, and *N. crucifera*, respectively). *Verrucosa arenata* values were compared with a t test, whereas the other species were compared with Wilcoxon tests, because one or more values were not

normally distributed. Therefore, the hypothesis that repeated cycling drew aqueous material from a droplet was refuted, and any change in droplet volume must be explained by another mechanism.

Droplet extension length

Mean filament length at pull-off shortens after 40 cycles in most treatments (Table 1, Tables 5-8). This occurs at both humidities in *V. arenata* and *L. cornutus* and at low humidity in *A. aurantia*. However, cycling did not decrease filament length for *A. aurantia* at high humidity or *N. crucifera* at either humidity. To create an index of droplet extension length that was not affected by the variability in the length of focal extension 1, we determined the deviation of each individual's droplet length at pull-off from the mean lengths of the eight focal extensions. These values typically decreased during cycling (Figures 5 and 6). However, in *N. crucifera*, at low humidity, there was no change in filament length, and, in *A. aurantia*, at high humidity, filament length appeared to increase (Figures 5d and 6a).

Force on droplet at pull-off and estimated work

Force on a droplet at pull-off only decreased after cycling in *N. crucifera* at low humidity, while it was unaffected in the remaining 7 treatments (Table 2). The estimated work required to extend the droplet to pull-off after cycling decreased in *A. aurantia* at low humidity, but not in other treatments (Table 2).

The effect of humidity on extension cycling

To determine if humidity affected the decline in filament length as a result of cycling, we compared the percent decrease in filament length after cycling at high and low humidities of each species. Humidity did not affect the decline in filament length after cycling for any of the species (Wilcoxon $P > 0.2207$ for *A. aurantia*, *Larinioides cornutus*, and *Neoscona crucifera*; t test $P = 0.3830$ for *V. arenata*). Thus, the hypothesis that humidity affects the performance of glycoprotein during cycling was not supported by droplet filament length.

Examination of droplet residue

FESEM examination revealed what we interpret to be several concentric rings of LMMC deposits and two small glycoprotein deposits following 40 droplet extensions (Figure 7). However, these deposits were not thick enough to allow elemental analyses.

Discussion:

Impact of cycling on droplet properties and performance

Previous studies have shown that viscous capture threads respond to changes in environmental humidity (Opell et al. 2018a, b). The current study's results support the hypothesis that orb weaver capture spiral droplets are capable of extensive cycling, a performance characteristic that is widely associated with a smart material (Hebda and White 1995; Talbot 2003; Smith 2006). However, the hypothesized greater decrease in droplet performance at low humidity was not supported. Many droplet characteristics did not change in response to cycling, showing that capture droplets are still functional after extensive reuse. The most pronounced and consistent change associated with cycling was a reduction in filament length at pull-off.

Glycoprotein surface area remained unchanged or, in *A. aurantia*, increased at both humidities. The force on a droplet filament at pull-off remained unchanged in all but *N. crucifera* at low humidity. Taken together, these observations indicate that cycling increases the cohesion of a droplet's glycoprotein, such that pull-off force is reached at shorter filament length. Another expression of this increased glycoprotein cohesion is the ability of a droplet to return to its initial symmetrical, ellipsoid configuration. After extensive cycling, many droplets became asymmetrical and did not regain their original shape (Figure 4), indicating that their glycoprotein cores were stiffer.

Another notable effect of cycling was the decrease in droplet volume. Measurements of inter-droplet diameter do not support the flow of aqueous material out of the droplet and require another explanation. The presence of suspected LMMCs and glycoprotein residues on a surface after 40 droplet cycles suggests another mechanism. Comparison of glycoprotein volume before and after cycling does not suggest that glycoprotein loss accounts for a reduction in filament length. However, the presence of

putative LMMC deposits could explain the reduction in a droplet's aqueous volume after cycling as well as an increase in glycoprotein cohesion, because LMMCs contribute to both droplet hygroscopicity and glycoprotein plasticity. Although it is not possible to rule out evaporative water loss from droplets during cycling, this loss of LMMCs is a compelling explanation of our findings that is consistent with a developing understanding of the key role that LMMCs play in droplet performance (Townley and Tillinghast 2013; Amarpuri et al. 2015a, b; Singla et al. 2018). A contributing factor may have been that repeated droplet–probe contact compressed the glycoprotein, compacting its molecules and causing it to stiffen.

A surprising observation was how securely a droplet's glycoprotein core remained attached to the flagelliform axial fibers through cycling. In only four out of forty-four treatments did this anchor fail and droplets remain attached to the probe tip. In all cases of droplet detachment, when the naked flagelliform fibers were brought into contact with the droplet, which adhered to the probe, the droplet extended and at pull- off again remained attached to the probe. These observations are consistent with the presence of an anchoring granule at the center of a droplet that firmly, but not permanently, secures the glycoprotein mass to the flagelliform fibers (Opell and Hendricks 2010). In preparing focal droplets, we were able to slide adjacent droplets with no noticeable effect other than these droplets merging to form a larger droplet. Reattachment of droplets to flagelliform fibers suggests that a droplet's granule may represent a configurational change in glycoprotein as it interacts with flagelliform fiber binding sites and not another protein component in a droplet's glycoprotein core.

What do the results mean for natural capture thread function?

Our study characterized cycling of single droplets on a smooth surface. In nature, insects contact multiple droplets with surfaces of different textures. Surface texture is known to affect viscous thread adhesion (Opell and Schwend 2007). However, it is likely that our findings would apply at these higher levels, although it is unlikely that droplets would naturally experience the extensive cycling we employed. The ability of viscous droplets to cycle is useful for orb weavers because it allows droplets to function after initial pull-off, when a struggling insect re-contacts a droplet. In the context of the

suspension bridge system, the outer droplets of an adhering thread span contribute the most adhesive force and are typically the first to pull off (Opell and Hendricks 2009). Consequently, if these outer droplets can reattach, the suspension bridge would be reestablished. Although droplet filament length and volume decrease with repeated use, the limited changes in force and estimated work after a single extension would not substantially decrease prey retention. For subsequent insects, cycling may not be relevant. When insects are trapped in an orb web, they either escape or are subdued by the spider, both of which result in significant damage to the capture threads. This structural damage may reduce cycling's usefulness in subsequent insect capture.

Conclusion:

Viscoelastic orb weaver droplets are able to repeatedly adhere, extend, and pull off from a surface. This cycling, combined with their environmental response to humidity, classifies orb weaver droplets as smart materials. The capture thread has already been shown to function as a liquid–solid hybrid material when extended and compressed, and this study further documents the unique material properties of capture spiral silk (Elettro et al. 2015, 2016). Extension cycling comes at a cost of reduced filament length, increased glycoprotein cohesion, and reduced aqueous layer volume, but a droplet's glycoprotein contact area, force at pull-off, and estimated work of extension remain unchanged after extensive reuse. It has been well documented that droplets absorb atmospheric humidity, with volume, filament length, and glycoprotein thickness changing significantly with changing relative humidity (Opell et al. 2018a, b). However, relative humidity does not appear to change how droplets of most species respond to cycling. Cycling allows for the spider to rely on its capture droplets after initial pull-off, increasing spider capture efficiency. The reusability of these droplets is remarkable because it requires all internal components of the droplet to continue their elaborate interactions, many of which we do not fully understand. This durability is also an important characteristic for glycoprotein mimicking adhesives. Not only are orb weaver droplets self-assembled aqueous glues made in ambient conditions (instead of factories), but these adhesives are also reusable, indicating that glycoprotein mimicking adhesives could be significantly more eco-friendly than existing industry adhesives.

Acknowledgments: We would like to acknowledge Stephen McCartney for his assisted use of the LEO FESEM at Virginia Tech's Nanoscale Characterization and Fabrication Laboratory.

Funding support: We would like to acknowledge the National Science Foundation for funding this study (grant IOS-1257719).

Compliance with ethical standards

Competing interests: The authors declare that they have no competing interests in this study.

Chapter 2 Figures

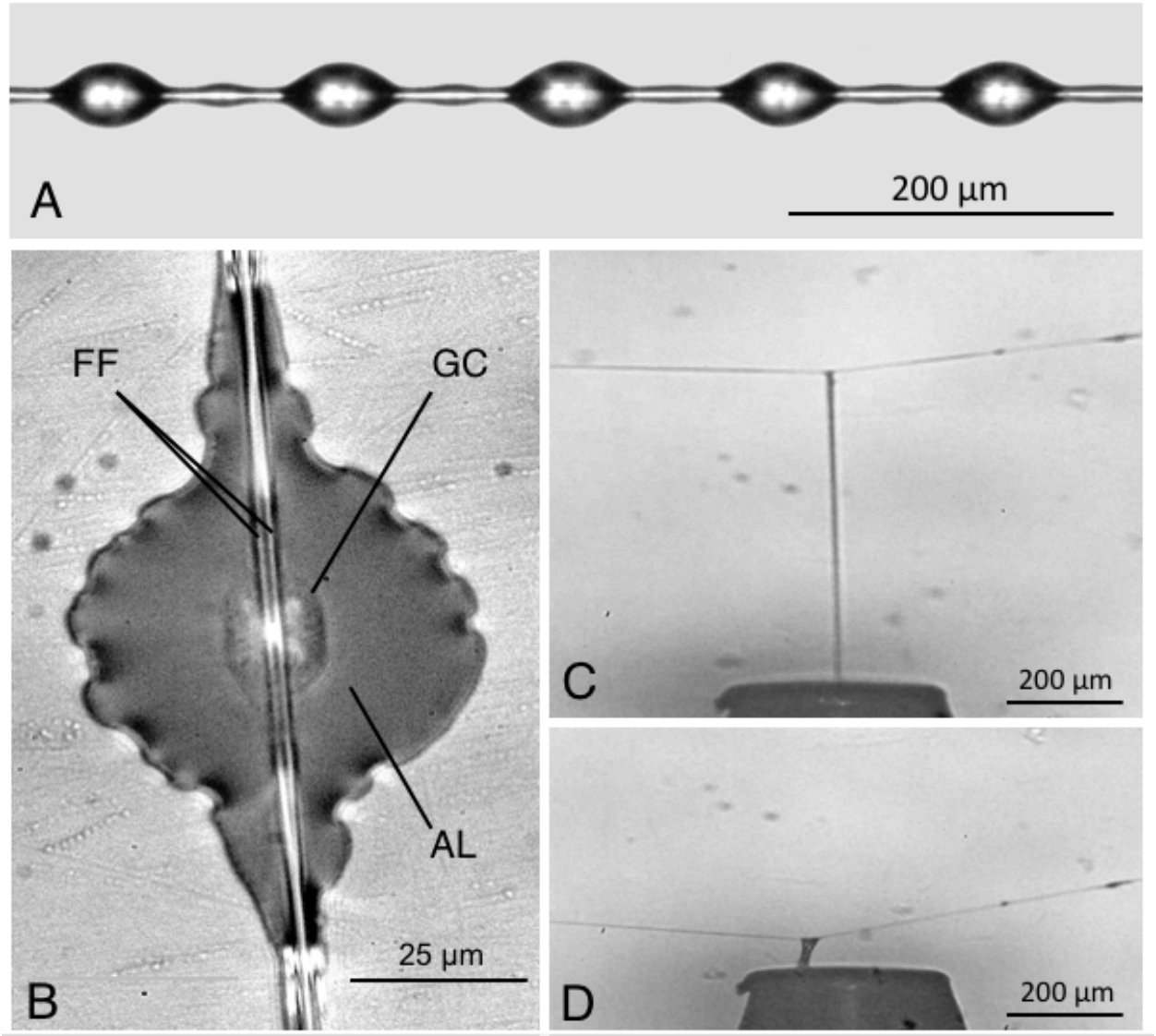

Figure 1: Orb web capture thread and droplet features. A. Capture thread strand with viscous glue droplets. B: Flattened droplet, showing a pair of flagelliform fibers (FF), glycoprotein core (GC), and aqueous layer (AL). C. Extended droplet filament just before pull-off at the first extension. D. The same droplet at pull-off at fortieth extension.

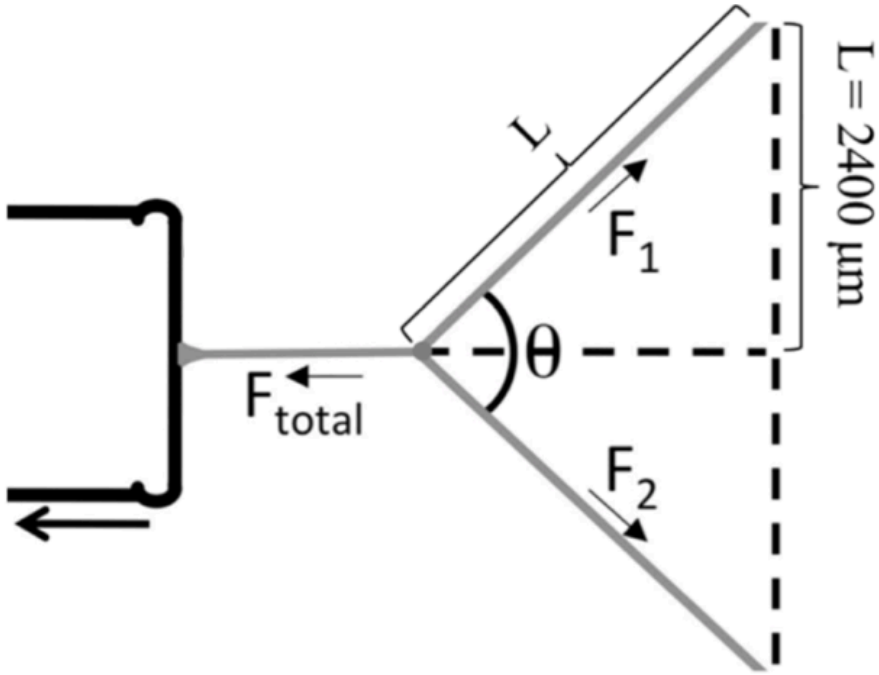

Figure 2: Diagram visualizing how force on a droplet at pull-off is calculated.

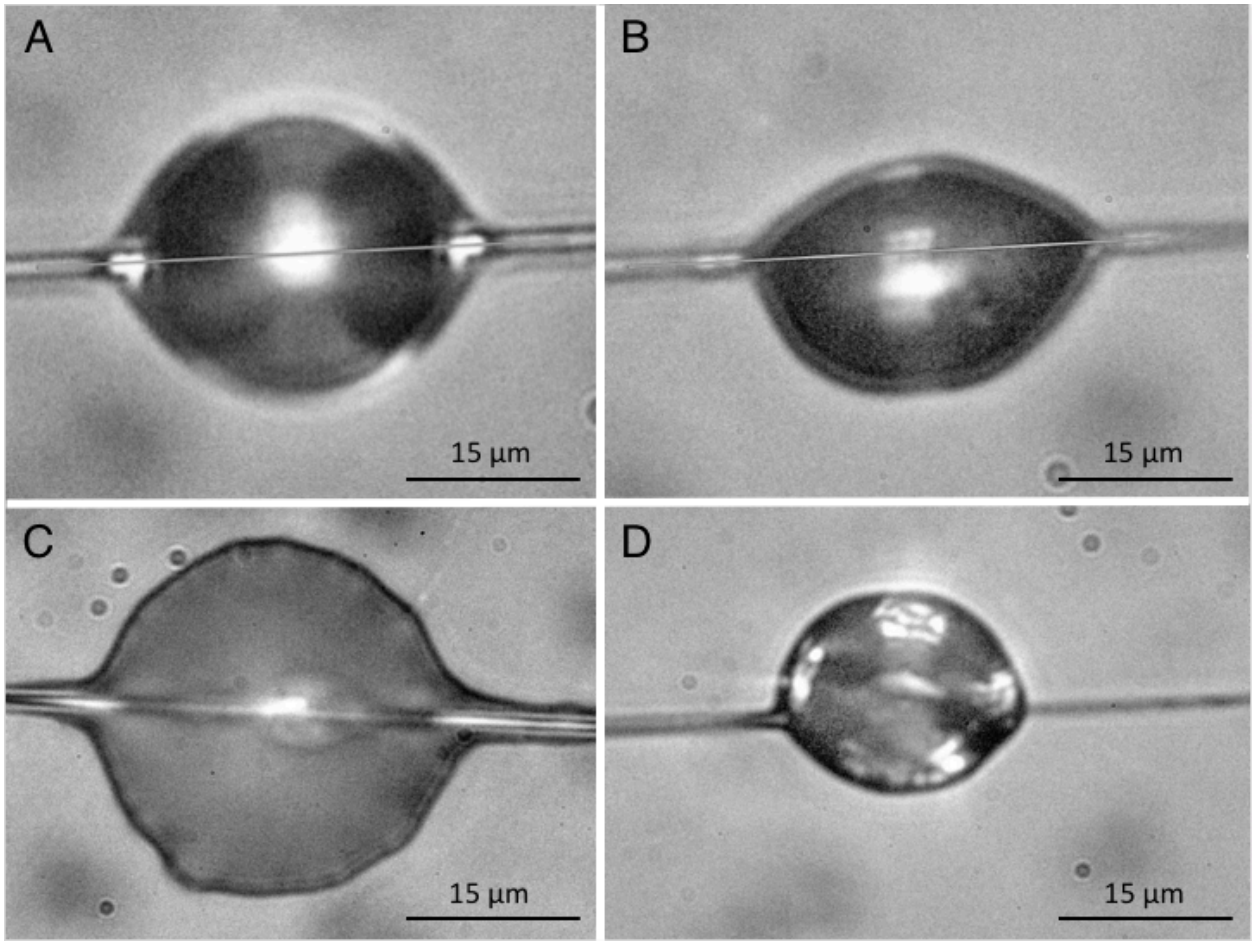

Figure 3: The effect of cycling on droplet volume, symmetry, and glycoprotein surface area. A. A suspended V. arenata droplet before cycling. B: The same droplet after 40 extension cycles, noticeably asymmetrical. C: A flattened V. arenata reference droplet. D: The same droplet after 40 extension cycles.

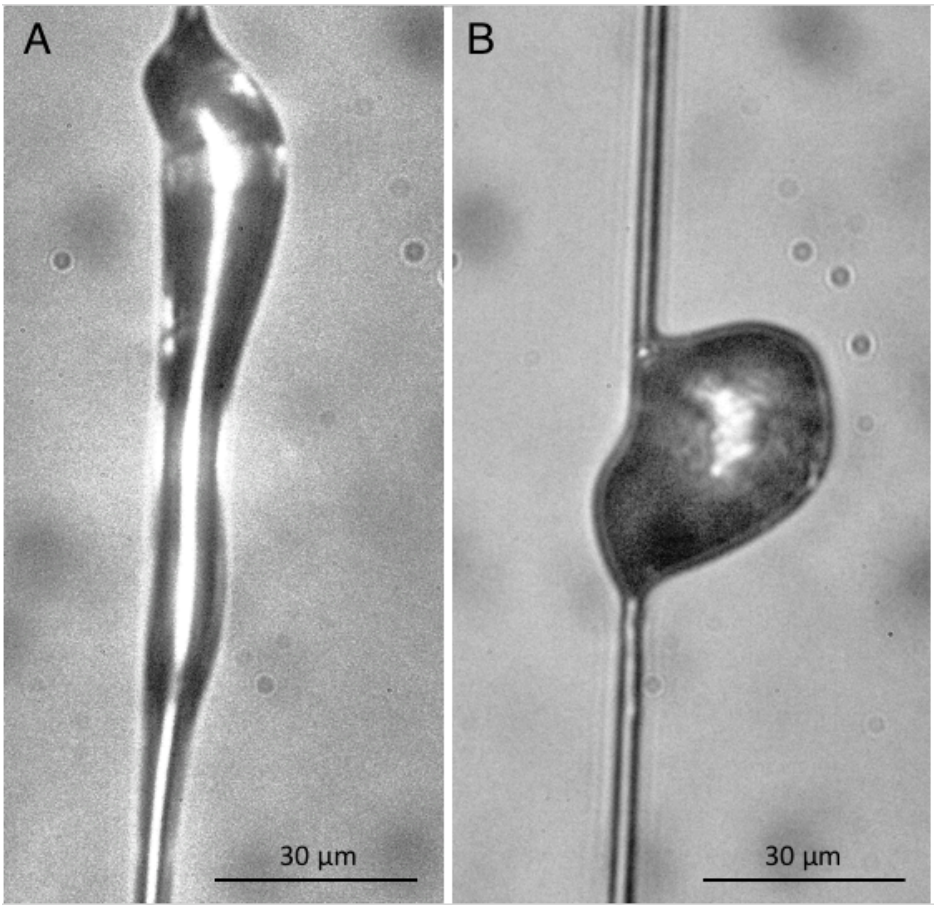

Figure 4: Two highly deformed droplets after cycling. Droplets such as these were rare but required volumes to be determined as a combination of cylinders and cones.

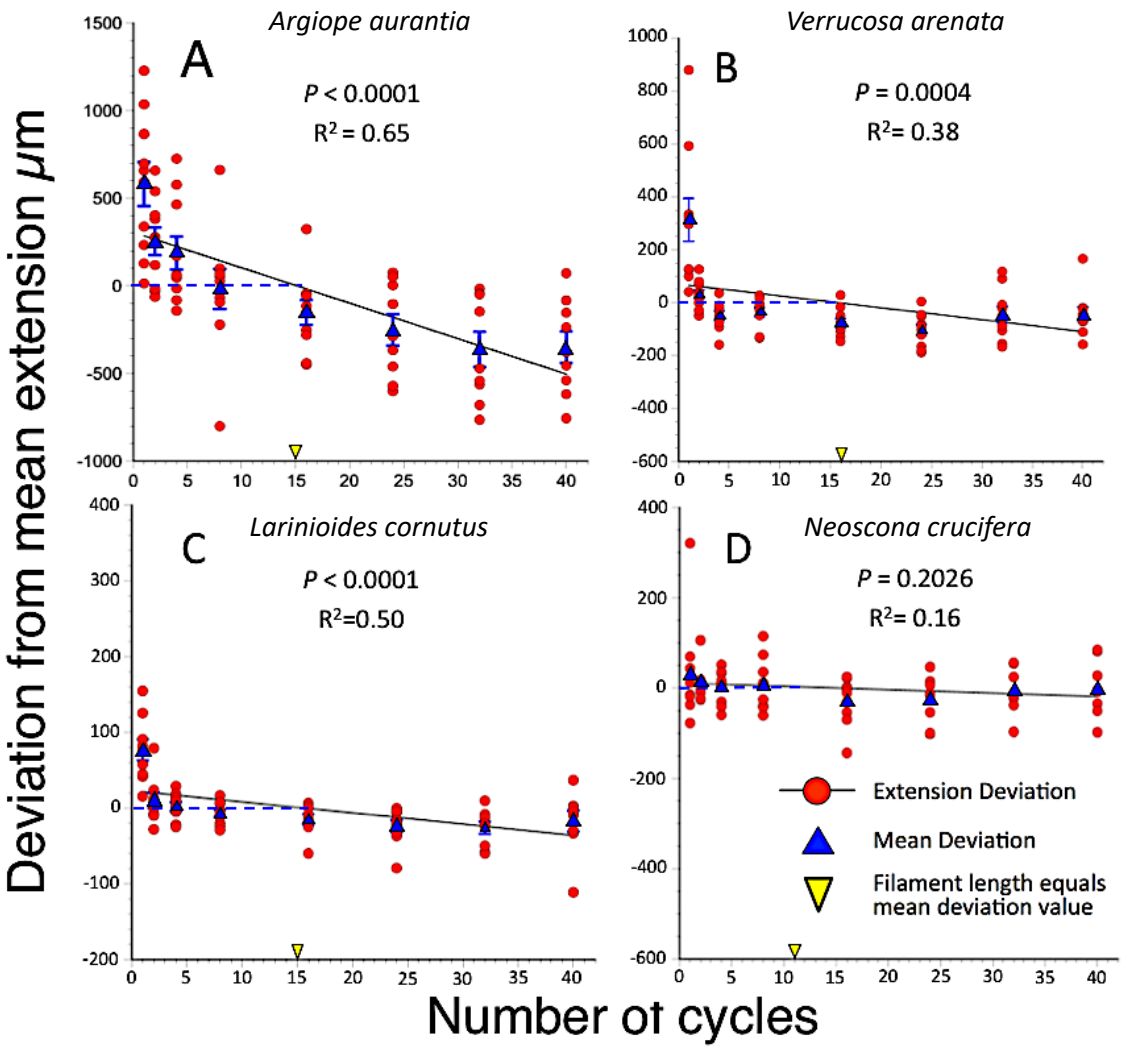

Figure 5: Filament lengths at focal extensions at low humidity expressed as deviations from mean extension length. *Neoscona crucifera* (5D) is the only species at this humidity where this relationship is not negative.

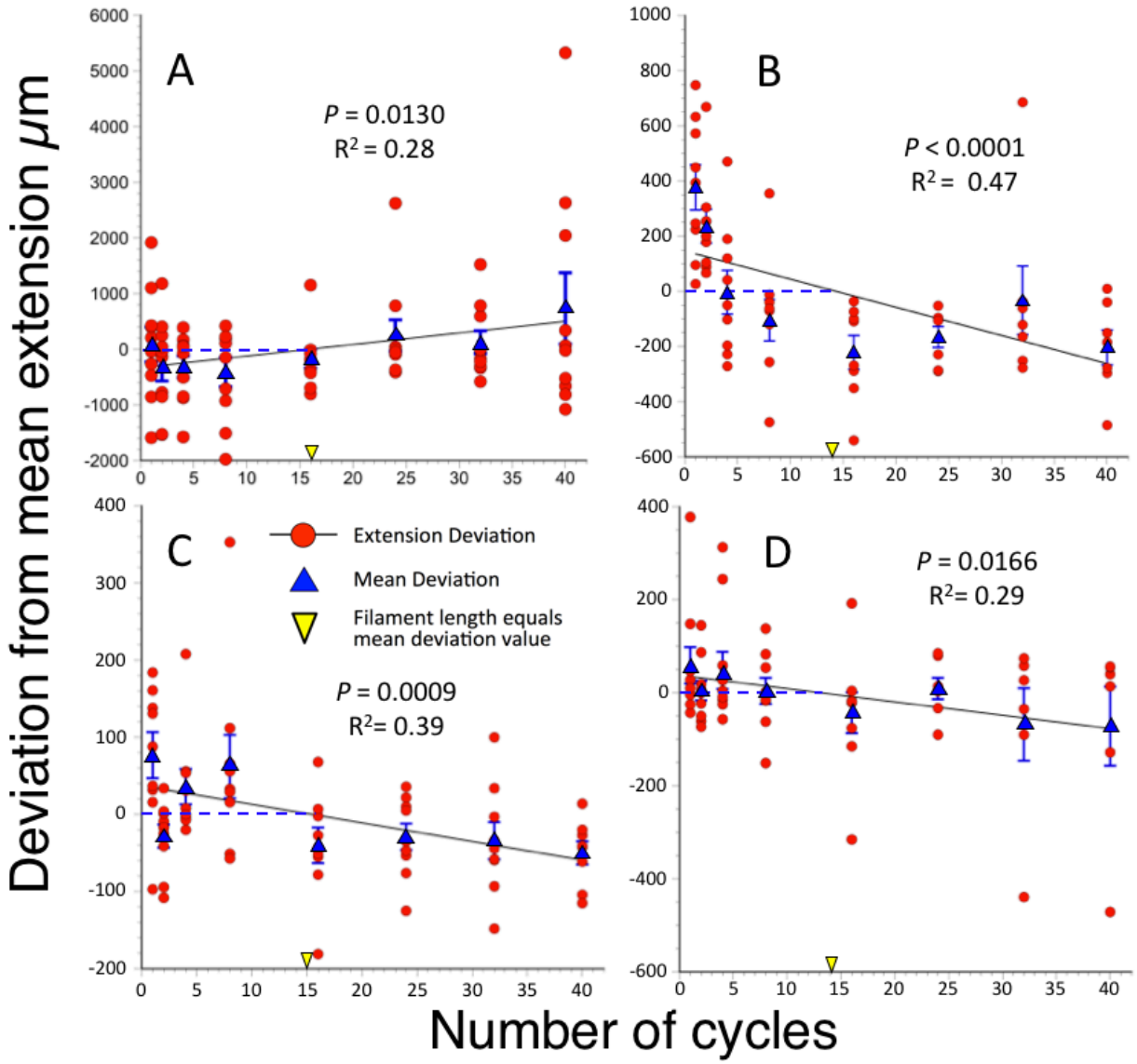

Figure 6: Filament lengths at focal extensions at high humidity expressed as deviations from mean extension length. *Argiope aurantia* (6A) is the only species at this humidity where this relationship is not negative. Species are *A. aurantia* (A), *V. arenata* (B), *L. cornutus* (C), and *N. crucifera* (D).

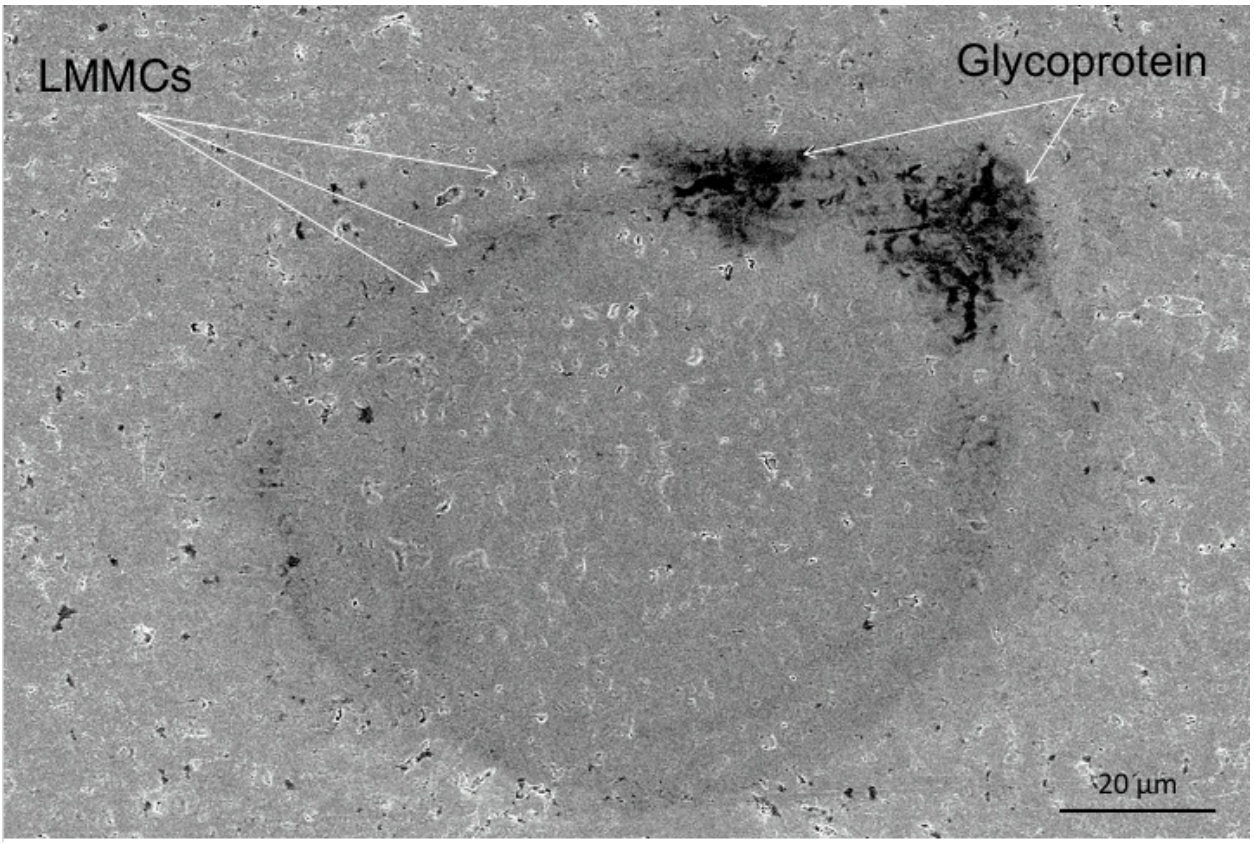

Figure 7: A scanning electron micrograph photograph showing putative LMMCs and glycoprotein residues left on a steel surface after 40 extension cycles of a *L. cornutus* droplet.

Chapter 2 tables

		Mean extension length (μm)		Matched pairs difference of extension lengths	
Species	Humidity	Fresh	Cycled	Standard error	P value
Argiope aurantia (10)	Low RH	1617	649	± 215	0.0020
	High RH	1831	2480	± 913	0.4956
Verrucosa arenata (10)	Low RH	537	180	± 86	0.0024
	High RH	779	186	± 130	0.0039
Larinioides cornutus (11)	Low RH	194	100	± 27	0.0079
	High RH	315	184	± 35	0.0072
Neoscona crucifera (9)	Low RH	236	210	± 60	0.6709
	High RH	362	200	± 147	0.3207
		Mean droplet volume (μm^3)		Matched pairs difference of droplet volumes	
Species	Humidity	Fresh	Cycled	Standard error	P value
Argiope aurantia (10)	Low RH	43612	33441	± 1908	0.0005
	High RH	51358	35839	± 3361	0.0013
Verrucosa arenata (10)	Low RH	10021	9115	± 986	0.3820
	High RH	12138	9070	± 1136	0.0356
Larinioides cornutus (11)	Low RH	6245	5108	± 474	0.0433
	High RH	8000	5834	± 523	0.0032
Neoscona crucifera (9)	Low RH	21279	15057	± 3154	0.0891
	High RH	12661	8850	± 1089	0.0173
		Mean Symmetry index		Matched pairs difference of symmetry	
Species	Humidity	Fresh	Cycled	Standard error	P value
Argiope aurantia (10)	Low RH	0.98	0.59	± 0.07	0.0003
	High RH	0.98	0.74	± 0.05	0.0009
Verrucosa arenata (10)	Low RH	0.96	0.68	± 0.05	0.0004
	High RH	0.96	0.68	± 0.07	0.0058
Larinioides cornutus (11)	Low RH	0.99	0.64	± 0.04	0.001
	High RH	0.94	0.67	± 0.07	0.0026
Neoscona crucifera (9)	Low RH	0.94	0.60	± 0.08	0.0047
	High RH	0.96	0.67	± 0.08	0.0195

Table 1: Droplet metrics that decrease with cycling. These consistent decreases in extension length, droplet volume, and symmetry support the hypothesis that cycling alters droplets. *P* values under 0.05 are in bold and were interpreted as significant.

		Estimated work (J)		Matched pairs difference of work	
Species	Humidity	Fresh	Cycled	Standard error	*P* value
Argiope aurantia (10)	Low RH	7.22×10^7	3.01×10^7	$\pm 1.75 \times 10^7$	**0.0427**
	High RH	4.47×10^7	1.69×10^8	$\pm 8.16 \times 10^7$	0.1659
Verrucosa arenata (10)	Low RH	1.99×10^6	1.38×10^6	7.92×10^5	0.4613
	High RH	5.20×10^6	1.12×10^6	3.30×10^6	0.2707
Larinioides cornutus (11)	Low RH	4.85×10^5	2.15×10^5	1.35×10^5	0.0805
	High RH	4.87×10^5	4.57×10^5	1.55×10^5	0.8538
Neoscona crucifera (9)	Low RH	1.91×10^7	1.47×10^7	8.57×10^6	0.6248
	High RH	2.89×10^6	7.00×10^6	3.14×10^6	0.2481
		Adhesive force (μN)		Matched pairs difference of work	
Species	Humidity	Fresh	Cycled	Standard error	*P* value
Argiope aurantia (10)	Low RH	6.175	24.36	12.084	0.1806
	High RH	1.135	6.747	4.208	0.2151
Verrucosa arenata (10)	Low RH	6.864	4.507	5.644	0.6861
	High RH	27.322	16.507	6.788	0.0983
Larinioides cornutus (11)	Low RH	4.893	3.881	1.136	0.3990
	High RH	8.287	10.386	2.142	0.3559
Neoscona crucifera (9)	Low RH	17.943	11.887	3.083	**0.0380**
	High RH	27.399	29.94	4.567	0.7232

Table 2: Table comparing droplet performance at the initial (fresh) cycle versus final cycle in terms of the force required to extend a droplet and the estimated work required to do so. Here, matched pairs analysis does not find evidence to support the hypothesis of decreased droplet performance due to cycling.

		Mean droplet volumes compared		Difference between droplets	Matched pairs difference between volumes	
Species	Humidity	Reference	Fresh	Absolute value	Standard error	*P* value
Argiope aurantia (10)	Low RH	42424	43612	1188	2929	0.6946
	High RH	48674	51358	2684	2424	0.2969
Verrucosa arenata (10)	Low RH	9612	10021	409	824	0.6861
	High RH	11036	10993	10.82	576	0.9412
Larinioides cornutus (11)	Low RH	6514	6245	269	1074	0.8086
	High RH	5431	8000	2569	701	**0.0063**
Neoscona crucifera (9)	Low RH	15677	19728	4051	2438	0.1352
	High RH	12768	14612	1844	1867	0.3523

Table 3: "Fresh" droplets are cycled droplet before their trials and reference droplets are droplets from the same web that allow for a comparison of glycoprotein characters. In all cases but one, the mean volumes between droplets of the same web did not differ.

		Thickness (μm)		Matched pairs difference between thickness	
Species	Humidity	Reference	Cycled	Standard error	*P* value
Argiope aurantia (10)	Low RH	5.536	5.467	0.401	0.4760
	High RH	4.536	4.779	0.200	0.3180
Verrucosa arenata (10)	Low RH	3.003	3.213	0.191	0.3004
	High RH	3.031	3.489	0.875	0.8257
Larinioides cornutus (11)	Low RH	3.438	4.131	1.022	0.5165
	High RH	2.072	2.819	0.225	**0.0105**
Neoscona crucifera (9)	Low RH	9.641	9.459	1.950	0.5849
	High RH	4.286	9.5	1.257	0.1689
		Glycoprotein volume (μm^3)		Matched pairs difference between volumes	
Species	Humidity	Reference	Cycled	Standard error	*P* value
Argiope aurantia (10)	Low RH	7033	8715	1153	0.1826
	High RH	5431	9805	1432	**0.0157**
Verrucosa arenata (10)	Low RH	1471	2129	474	0.1984
	High RH	1141	1892	336	0.0756
Larinioides cornutus (11)	Low RH	682	601	140	0.5791
	High RH	483	768	134	0.0664
Neoscona crucifera (9)	Low RH	3957	5025	1562	0.5165
	High RH	2513	3188	735	0.4006
		Glycoprotein surface area (μm^3)		Matched pairs difference between areas	
Species	Humidity	Reference	Cycled	Standard error	*P* value
Argiope aurantia (10)	Low RH	1249	1516	115	**0.0447**
	High RH	1198	2044	304	**0.0237**
Verrucosa arenata (10)	Low RH	550	665	164	0.5017
	High RH	368	591	116	0.0965
Larinioides cornutus (11)	Low RH	196	171	27	0.3720
	High RH	228	299	44	0.1477
Neoscona crucifera (9)	Low RH	323	491	76	0.0573
	High RH	679	399	317	0.4102

		Glycoprotein ratio		Matched pairs difference between ratios	
Species	Humidity	Reference	Cycled	Standard error	*P* value
Argiope aurantia (10)	Low RH	0.15	0.25	0.033	**0.0126**
	High RH	0.11	0.26	0.042	**0.0066**
Verrucosa arenata (10)	Low RH	0.16	0.26	0.034	**0.0161**
	High RH	0.09	0.27	0.045	**0.0052**
Larinioides cornutus (11)	Low RH	0.11	0.11	0.013	0.8794
	High RH	0.08	0.13	0.010	**0.0018**
Neoscona crucifera (9)	Low RH	0.19	0.35	0.050	**0.0122**
	High RH	0.26	0.37	0.080	0.2368

Table 4: Using references droplets, we were able to compare glycoprotein between cycled and uncycled droplets. Glycoprotein ratio = glycoprotein volume/droplet volume. The increase in glycoprotein ratio after cycling indicates a decrease in aqueous layer volume. Parentheses indicate sample size.

**Tables were originally supplementary figures in Kelly et al. 2019 and are cited as Tables 5-8 in Chapter 2.*

Argiope aurantia (N = 10) Focal extension	Mean Filament Length µm		Mean Droplet volume μm^3	
	37% RH	55% RH	37% RH	55% RH
1	1536 ± 273	1831 ± 340	33812 ± 3315	36490 ± 5275
2	1211 ± 199	1450 ± 279	29877 ± 3059	36329 ± 5864
4	1144 ± 227	1431 ± 264	29608 ± 2630	38376 ± 6310
8	938 ± 173	1336 ± 205	32350 ± 3227	38164 ± 6588
16	805 ± 149	1580 ± 309	32890 ± 3144	36801 ± 6253
24	748 ± 145	1993 ± 529	35689 ± 5169	35521 ± 7674
32	636 ± 119	1875 ± 436	35636 ± 4311	33927 ± 6651
40	649 ± 117	2480 ± 824	34074 ± 4730	35839 ± 8114

Table 5: *Argiope aurantia* mean filament length and droplet volume thorough cycling with standard error.

Verrucosa Arenata (N = 10) Focal extension	Mean Filament Length µm		Mean Droplet volume μm^3	
	55% RH	72% RH	55% RH	72% RH
1	537 ± 100	785 ± 116	8845 ± 1072	7593 ± 2018
2	256 ± 17	672 ± 97	8854 ± 1269	7068 ± 2241
4	175 ± 14	409 ± 134	8809 ± 1284	7863 ± 1989
8	189 ± 27	310 ± 77	9255 ± 1095	7917 ± 1804
16	147 ± 18	167 ± 42	9357 ± 1125	8979 ± 1951
24	121 ± 13	236 ± 61	9143 ± 1095	8998 ± 2264
32	179 ± 38	395 ± 207	9248 ± 1181	9049 ± 2148
40	180 ± 44	206 ± 38	9115 ± 1585	8871 ± 2165

Table 6: *Verrucosa arenata* mean filament length and droplet volume thorough cycling with standard error.

Larinioides cornutus (N = 9) Focal extension	Mean Filament Length µm		Mean Droplet volume μm^3	
	55% RH	72% RH	55% RH	72% RH
1	194 ± 26	304 ± 40	6677 ± 1343	8541 ± 1947
2	127 ± 22	199 ± 25	6625 ± 1365	8098 ± 1942
4	119 ± 20	263 ± 49	6667 ± 1268	7983 ± 1879
8	110 ± 16	289 ± 68	6544 ± 1388	8277 ± 1917
16	102 ± 15	187 ± 31	6421 ± 1377	7752 ± 1948
24	93 ± 10	198 ± 28	6611 ± 1370	7868 ± 2041
32	91 ± 10	193 ± 36	6253 ± 1346	7396 ± 1857
40	100 ± 14	184 ± 23	6480 ± 1314	6901 ± 1559

Table 7: *Larinioides cornutus* mean filament length and droplet volume thorough cycling with standard error.

Neoscona crucifera (N = 11) Focal extension	Mean Filament Length µm		Mean Droplet volume μm^3	
	55% RH	72% RH	55% RH	72% RH
1	251 ± 56	373 ± 83	16813 ± 6407	15106 ± 5277
2	232 ± 34	320 ± 63	15742 ± 5376	15246 ± 5264
4	222 ± 29	363 ± 78	15758 ± 5847	15033 ± 5257
8	229 ± 36	345 ± 70	14165 ± 4743	10240 ± 2735
16	191 ± 26	299 ± 73	13252 ± 3942	10071 ± 2480
24	183 ± 33	305 ± 65	15367 ± 5265	11390 ± 3081
32	204 ± 33	234 ± 31	14966 ± 5280	9055 ± 2782
40	210 ± 35	234 ± 26	15057 ± 5574	8740 ± 2597

Table 8: *Neoscona crucifera* mean filament length and droplet volume thorough cycling with standard error.

References

Adams MR (2000) Choosing Hunting Sites: Web Site Preferences of the Orb Weaver Spider, Neoscona crucifera, Relative to Light Cues. J Insect Behav 13:299–305

Amarpuri G, Chaurasia V, Jain D, et al (2015a) Ubiquitous distribution of salts and proteins in spider glue enhances spider silk adhesion. Sci Rep 5:. https://doi.org/10.1038/srep09030

Amarpuri G, Zhang C, Diaz C, et al (2015b) Spiders Tune Glue Viscosity to Maximize Adhesion. Am Chem Soc 9:11472–11478. https://doi.org/10.1021/acsnano.5b05658

Ayoub NA, Garb JE, Tinghitella RM, et al (2007) Blueprint for a High-Performance Biomaterial: Full-Length Spider Dragline Silk Genes. PLoS One 2:e514. https://doi.org/https://doi.org/10.1371/journal.pone.0000514

Blackledge TA, Eliason CM (2007) Functionally independent components of prey capture are architecturally constrained in spider orb webs. Biol Lett 3:. https://doi.org/https://doi.org/10.1098/rsbl.2007.0218

Blackledge TA, Hayashi CY (2006) Silken toolkits: biomechanics of silk fibers spun by the orb web spider Argiope argentata (Fabricius 1775). J Exp Biol 209:2452–2461. https://doi.org/10.1242/jeb.02275

Blackledge TA, Scharff N, Coddington JA, et al (2009) Reconstructing web evolution and spider diversification in the molecular era. PNAS 106:5229–5234. https://doi.org/www.pnas.orgcgidoi10.1073pnas.0901377106

Bond JE, Opell BD (1998) Testing Adaptive Radiation and Key Innovation Hypothesis in Spiders. Evolution (N Y) 52:403–414

Bradley RA (2013) Common Spiders of North America. University of Califronia Press, Berkeley, CA

Carrel JE (2008) The effect of season of fire on density of female garden orbweavers (Araneae: Araneidae: Argiope) in Florida scrub. Florida Entomol 91:332

Choresh O, Bayarmagnai B, Lewis R V (2009) Spider Web Glue: Two Proteins Expressed from Opposite Strands of the Same DNA Sequence. Biomacromolecules 10:2852–2856. https://doi.org/10.1021/bm900681w

Coddington JA (1989) Spinneret Silk Spigot Morphology: Evidence for the Monophyly of Orbweaving Spiders, Cyrtophorinae (Araneidae), and Group Theridiidae plus Nesticidae. J Arachnol 17:71–95

Collin MA, Ayoub NA, Hayashi C (2016) Evidence from Multiple Species that Spider Silk Silk Glue Component ASG2 is a Spidroin. Sci Rep 6:. https://doi.org/10.1038/srep21589

Concha A, Mellado P, Morera-Brenes B, et al (2015) Oscillation of the velvet worm slime jet by passive hydrodynamic instability. Nat Commun 6:. https://doi.org/10.1038/ncomms7292

Dickinson GH, Vega IE, Wahl KJ, et al (2009) Barnacle cement: a polymerization model based on evolutionary concepts. J Exp Biol 212:3499–3510

Edmonds DT, Vollrath F (1992) The Contribution of Atmospheric Water Vapour to the Formation and Efficiency of a Spider's Capture Web. R Soc 248:145–148. https://doi.org/10.1098/rspb.1992.0055

Elbaum R, Zaltzman L, Burgert I, Fratzl P (2007) The Role of Wheat Awns in the Seed Dispersal Unit. Science (80-) 316:884–886.

https://doi.org/10.1126/science.1140097
Elettro H, Neukirch S, Antkowiak A, Vollrath F (2015) Adhesion of dry and wet electrostatic capture silk of uloborid spider. Sci Nat 102:. https://doi.org/10.1007/s00114-015-1291-6
Elettro H, Neukirch S, Vollrath F, Antkowiak A (2016) In-drop capillary spooling of spider capture thread inspires hybrid fibers with mixed solid–liquid mechanical properties. PNAS 113:6143–6147
Enders F (1977) Web-site Selection by Orb-web Spiders, particularly Argiope aurantia (Lucas). Anim Behav 25:694–712
Foelix RF (2011) Biology of Spiders, 3rd edn. Oxford Univeristy Press, New York, NY
Gaddy LL (1987) Orb-Weaver Abundance in Three Forested Communities in the Southern Appalacian Mountains of South Carolina. J Arachnol 15:273–275
Garb JE, Ayoub NA, Hayashi C (2010) Untangling spider silk evolution with spidroin terminal domains. BMC Evol Biol 10:. https://doi.org/10.1186/1471-2148-10-243
Gatesy J, Hayashi C, Motriuk D, et al (2001) Extreme Diversity, Conservation, and Convergence of Spider Silk Fibroin Sequences. Science (80-) 291:2603–2605. https://doi.org/10.1126/science.1057561
Hebda DA, White SR (1995) Effect of training conditions and extended thermal cycling on nitinol two-way snape memory benavior. Smart Mater Struct 4:298–304
Hoogenboom R (2014) Temperature-responsive polymers: properties, synthesis and applications. In: Román JS (ed) Smart Polymers and their Applications. Woodhead Publishing, Cambridge, pp 15–44
Huang Y, Wang Y, Sun L, et al (2015) Sundew adhesive: a naturally occurring hydrogel. J R Soc Interface 12:. https://doi.org/10.1098/rsif.2015.0226
Jain D, Sahni V, Dhinojwala A (2014) Synthetic Adhesive Attachment Discs Inspired by Spider's Pyriform Silk Architecture. J Polym Sci Part B Polym Phys 52:553–560. https://doi.org/10.1002/polb.23453
Jensen RA, Morse DE (1988) The bioadhesive of Phragmatopoma californica tubes: a silk-like cement containingL-DOPA. J Comp Physiol B 158:317–324. https://doi.org/https://doi.org/10.1007/BF00695330
Kamila S (2013) Introduction, classification and applications of smart materials: an overview. Am J Appl Sci 10:876–880. https://doi.org/10.3844/ajassp.2013.876.880
Kamino K (2010) Molecular design of barnacle cement in comparison with those of mussel and tubeworm. J Adhes 86:96–110
Li D, Huson MG, Graham LD (2008) Proteinaceous adhesive secretions from insects, and in particular the egg attachment glue of Opodiphthera sp. moths. Arch Insect Biochem Physiol 69:85–105. https://doi.org/10.1002/arch.20267
Liao C-P, Blamires SJ, Hendricks ML, Opell BD (2015) A re-evaluation of the formula to estimate the volume of orb web glue droplets. J Arachnol 43:97–100
Mackay RJ, Wiggins GB (1979) Ecological diversity in Trichoptera. Annu Rev Entomol 24:185–208
Mead-Hunter R, King AJC, Mullins BJ (2012) Plateau Rayleigh instability simulation. Langmuir 28:6731–6735
Naldrett MJ (1993) The importance of sulphur cross-links and hydrophobic interactions in the polymerization of barnacle cement. J Mar Biol Assoc 73:689–702
Opell BD, Clouse ME, Andrews SF (2018a) Elastic modulus and toughness of orb spider

glycoprotein glue. PLoS One 13:. https://doi.org/https://doi.org/10.1371/journal.pone.0196972
Opell BD, Hendricks ML (2007) Adhesive recruitment by the viscous capture threads of araneoid orb-weaving spiders. J Exp Biol 210:553–560. https://doi.org/doi:10.1242/jeb.02682
Opell BD, Hendricks ML (2010) The role of granules within viscous capture threads of orb-weaving spiders. J Exp Biol 213:339–346. https://doi.org/10.1242/jeb.036947
Opell BD, Hendricks ML (2009) The adhesive delivery system of viscous capture threads spun by orb-weaving spiders. J Exp Biol 212:3026–3034. https://doi.org/10.1242/jeb.030064
Opell BD, Jain D, Dhinojwala A, Blackledge TA (2018b) Tuning orb spider glycoprotein glue performance to habitat humidity. J Exp Biol 221:. https://doi.org/10.1242/jeb.161539
Opell BD, Karinshak SE, Sigler MA (2013) Environmental response and adaptation of glycoprotein glue within the droplets of viscous prey capture threads from araneoid spider orb-webs. J Exp Biol 216:3023–3034. https://doi.org/10.1242/jeb.084822
Opell BD, Schwend HS (2007) The effect of insect surface features on the adhesion of viscous capture threads spun by orb-weaving spiders. J Exp Biol 210:2352–2360
Opell BD, Sigler SEKMA (2011) Humidity affects the extensibility of an orb-weaving spider's viscous thread droplets. J Exp Biol 214:2988–2993. https://doi.org/10.1242/jeb.055996
Palacio MLB, Bhushan B (2012) Bioadhesion: a review of concepts and applications. R Soc 370:2321–2347. https://doi.org/10.1098/rsta.2011.0483
Sahni V, Blackledge TA, Dhinojwala A (2011) Changes in the Adhesive Properties of Spider Aggregate Glue During the Evolution of Cobwebs. Sci Rep 1:1–8. https://doi.org/10.1038/srep00041
Sahni V, Dhinojwala A (2010) Viscoelastic solids explain spider web stickiness. Nat Commun 1:1–4. https://doi.org/10.1038/ncomms1019
Sahni V, Miyoshi T, Chen K, et al (2014) Direct Solvation of Glycoproteins by Salts in Spider Silk Glues Enhances Adhesion and Helps To Explain the Evolution of Modern Spider Orb Webs. Biomacromolecules 15:1225–1232. https://doi.org/10.1021/bm401800y
Sensenig AT, Agnarsson I, Blackledge TA (2010) Behavioral and biomaterial coevolution in spider orb webs. J Evol Biol 23:1839–1856. https://doi.org/10.1111/j.1420-9101.2010.02048.x
Sensenig AT, Kelly SP, Lorentz KA, et al (2013) Mechanical performance of spider orb webs is tuned for high-speed prey. J Exp Biol 216:3388–3394. https://doi.org/10.1242/jeb.085571
Sensenig AT, Lorentz KA, Kelly SP (2012) Spider orb webs rely on radial threads to absorb prey kinetic energy. J R Soc Interface 9:1880–1892
Singla S, Amarpuri G, Dhopatkar N, et al (2018) Hygroscopic compounds in spider aggregate glue remove interfacial water to maintain adhesion in humid conditions. Nat Commun 9:. https://doi.org/10.1038/s41467-018-04263-z
Smith R (2006) Smart Material Systems. Society for Industrial and Applied Mathematics, Philidelphia, pp 1–5
Talbot D (2003) Smart materials. 1–17

Tillinghast EK, Townley MA, Wight TN, et al (1993) The adhesive glycoprotein of the orb of Argiope aurantia (Araneae, Araneidae). Mater Res Soc Symp Proc 259:154–165

Townley MA, Bernstein DT, Gallagher KS, Tillinghast EK (1991) Comparative study of orb web hygroscopicity and adhesive spiral composition in three araneid spiders. J Exp Zool 259:154–165. https://doi.org/10.1002/jez.1402590203

Townley MA, Tillinghast EK (2013) Aggregate Silk Gland Secretions of Araneoid Spiders. Springer-Verlag Berlin Heidelberg

Vollrath F, Edmonds DT (1989) Modulation of the mechanical properties of spider silk by coating with water. Nature 340:305–307. https://doi.org/10.1038/340305a0

Vollrath F, Tillinghast EK (1991) Glycoprotein glue beneath a spider web's aqueous coat. Naturwissenschaften 78:557–559. https://doi.org/https://doi.org/10.1007/BF01134447

Waite HJ (2017) Mussel adhesion - essential footwork. J Exp Biol 220:517–530

Wolff JO, Grawe I, Wirth M, et al (2015) Spider's super-glue: thread anchors are composite adhesives with synergistic hierarchical organization. Soft Matter 11:2394–2403. https://doi.org/10.1039/c4sm02130d

Chapter 3: Biomechanics and evolution of the capture thread adhesive delivery system

**Preparing for submission*

Sean D. Kelly, Brent D. Opell, & Hannah Mae O. Elmore

ABSTRACT

Orb weavers intercept insects using non-hardening bioadhesive droplets, supported by two flagelliform fibers. Droplets contain an adhesive glycoprotein core and aqueous layer that confers hygroscopicity. However, adhesion is the result of an integrated performance of multiple droplets and the flagelliform fibers. As insects struggle, the flagelliform fibers bow and the droplets extend, forming a suspension bridge configuration whose biomechanics sum the adhesion of droplets and dissipate the energy of struggling insects. Given this performance, we predict that the material properties of both thread components have evolved in a complementary way. Comparative phylogenetics of 14 local orb weavers revealed that their elastic moduli are correlated, with glycoproteins being six times more elastic than flagelliform fibers. However, toughness displayed no evidence of synergy between the two components. Spider mass has been linked to capture thread performance, but comparative phylogenetics show that spider mass only affects the amount of each material, not their material properties. Since glycoprotein performance changes with humidity, we hypothesized that orb weavers generate the greatest adhesion at their foraging humidity. After delimiting low and high humidity species groups (eight and six species, respectively), bridge force was determined as total contributing droplet adhesion at three humidities. Only three spiders generated greater adhesion outside of their foraging humidity, providing evidence for habitat specialization in orb weavers. The distribution of force along a suspension bridge differs among species, contrary to a previously reported pattern. We also characterize the sheet configuration, which generates force similar to suspension bridges.

Introduction:

Adhesion in nature

Animals and plants rely on adhesion for many purposes. One use is in locomotion, where an adhesive (like gecko toe pads) allow an animal to resist gravity while climbing (Russell et al., 2019). Adhesive aid in locomotion is especially useful for arboreal leaf-cutter ants who must not only climb against gravity, but also carry heavy vegetation back to their colonies (Stark et al., 2019). Sea urchin locomotion is also assisted with adhesion, but here the adhesive functions underwater, resisting powerful waves and currents (Santos and Flammang, 2012; Santos et al., 2009). The nature of these adhesives is temporary, allowing an animal to generate and release adhesion as it moves over challenging terrain. This contrasts with adhesive anchoring, exhibited by barnacles and mussels. While the function is similar to sea urchins in that they resist the action of waves, these sessile animals use their adhesive to permanently anchor to wet and salt-encrusted surfaces (Dickinson et al., 2009; Waite, 2017). These adhesives allow animals to exploit their environment, but others use adhesion for protection. Notably, caddis fly larva and sandcastle worms shelter in tubes constructed from surrounding sediments (Wang et al., 2014; Zhao et al., 2016). A more dramatic example of a protective adhesive is the Cuvierian tubules in sea cucumbers. These tubules are secreted by mechanical stimulation and exhibit high stickiness and tensile strength, entangling and immobilizing potential predators (DeMoor et al., 2003). Yet another example of bioadhesion is in predation. Velvet worms use their oral papillae or “canons” to expel a sticky slime that rapidly solidifies onto an insect, preventing its escape (Corrales-Urena et al., 2017). Other adhesive prey capture is accomplished with non-hardening adhesives

that remain sticky after secretion. Often, these adhesives are employed by "sit and wait" predators that broadly distribute these adhesives, creating a trap for incoming prey that may strike it. Sundews use this strategy to supplement their nutrient intake, using leaves studded with glue droplet covered stalks (Huang et al., 2015). These plants have the added benefit that their glue droplets also act as lures, containing sugars that attract insects (Olivencia et al., 1995). The stimulus of a struggling insect causes the leaves bend inwards, bringing the insect closer to other sticky stalks and mechanically restraining it (Krausko et al., 2017). By using a glue that retains viscosity and is broadly distributed, sundews can generate a larger area for prey capture.

Orb weavers apply a similar strategy, using a broadly distributed and non-hardening glue in their orb webs (Sahni and Dhinojwala, 2010). However, two adhesives are required for a functional orb web. First, pyriform disks are used to anchor the web's major ampullate frame lines to nearby objects. Each disk is a zigzag array, overlaying the tougher frame line (Wolff and Gorb, 2016; Wolff et al., 2015). Changes in pyriform silk application in spiders has been linked to the diversification of various aerial webs and subsequent ecological success (Wolff et al., 2019). The second adhesive is used to ensnare insects that strike the web and forms the capture spiral thread. This adhesive thread features regularly spaced glue droplets supported by a pair of flagelliform fibers (Figure 1B) (Vollrath, 2000). Much like the closely packed glue stalks of sundews, the capture thread droplets work together to increase adhesion. During adhesion of the capture thread, droplet adhesive force is summed along the bowing flagelliform fiber pair, forming a suspension bridge configuration (Figure 1A) (Opell and Hendricks, 2007). This configuration sums the force of individual droplet extensions within a bridge,

generating greater adhesion with greater thread length (Opell and Hendricks, 2009). Simultaneously, the droplet's adhesive contributions are combined with the work done in extending the flagelliform fibers (Opell et al., 2008). Although initial research predicted that longer exterior bridge droplets would contribute more adhesion than the shorter interior droplets, a recent study showed the opposite (Opell and Stellwagen, 2019). While this aspect of the system may be variable, modeling reveals that suspension bridges are robust, with a random distribution of droplets not deteriorating adhesive loadbearing or energy absorption (Guo et al., 2019).

The objective of this study is to examine how individual droplet adhesion is integrated into the suspension bridge configuration and how humidity impacts this natural adhesive system. We investigated this with phylogenetic comparative methods using 14 orb weaving species that differ in body size and habitat. Among these spiders, we examined the evolutionary and functional relationships between flagelliform fibers and glycoprotein glue. Across this phylogeny of local species, we also examined the relationships between spider size and their capture thread components. Thus, our broad aim is to better understand how capture thread components are integrated biomechanically and how the adhesion they generate responds to environmental conditions.

The role of non-adhesive web elements

An orb web's anchor, frame, and radial lines are each composed of major ampullate silk (Blackledge and Hayashi, 2006). The greater diameters and stiffness of these threads better equips them to absorb the kinetic energy of flying insects, preventing

insects from bouncing off the web after impact (Sensenig et al., 2010; Sensenig et al., 2012; Swanson et al., 2006). This capability is highly conserved among orb weavers, reflecting its importance in orb web function and evolution (Kelly et al., 2011). Radial threads also send vibrations to the spider, allowing it to locate ensnared prey (Blackledge et al., 2011).

Capture thread formation and components

An orb web's capture spiral is suspended between adjacent radial threads and deposited from the perimeter to the center of the web (Foelix, 2011). A capture thread is a self-organizing adhesive. As they are spun, the supporting fibers are coated with aggregate gland solution (Coddington, 1989). This solution of proteins, low molecular mass compounds (LMMCs), and inorganic salts initially forms a cylinder around the flagelliform fiber pair. However, Plateau - Rayleigh instability quickly divides them into evenly spaced droplets (Figure 1B) (Edmonds and Vollrath, 1992; Mead-Hunter et al., 2012). The remaining material forms an aqueous layer that covers both the flagelliform fibers between droplets (Vollrath and Tillinghast, 1991). Within each droplet, a glycoprotein core forms and is responsible for its stickiness (Figure 1C) (Sahni and Dhinojwala, 2010; Tillinghast et al., 1993). Other amorphous proteins, which are not easily visualized, remain in the aqueous layer (Amarpuri et al., 2015a). While adhesion is the primary task of the droplets, they may also preserve the tension of the flagelliform fibers (Elettro et al., 2016).

The adhesive performance of the glycoprotein core is shaped by the LMMCs in the surrounding aqueous layer, with their concentration differing among species (Amarpuri et al., 2015b; Opell et al., 2018a). These compounds solvate the glycoprotein,

softening it and improving its adhesion (Sahni et al., 2014). Their other task is conferring hygroscopicity to the droplets, allowing droplet volume to track changes in atmospheric humidity. (Edmonds and Vollrath, 1992; Opell et al., 2018a; Townley et al., 1991). As water content increases, glycoprotein viscosity drops, and extensibility increases (Opell and Sigler, 2011; Opell et al., 2015). Optimal adhesion occurs when glycoprotein viscosity is low enough to establish a sufficient area of contact, but high enough to maintain glycoprotein cohesion during extension (Amarpuri et al., 2015b). The humidity where this occurs seems to match a species' foraging humidity, allowing orb weavers to occupy a range of habitats (Opell et al., 2013; Opell et al., 2018b). However, LMMC concentration alone may not determine droplet hygroscopicity, as these compounds interact with a droplet's proteins (Jain et al., 2018). Natural selection may tune droplet hygroscopicity to optimize insect retention times for an orb weaver's foraging humidity (Opell et al., 2017; Opell et al., 2019). The latter study also confirms that, as the suspension bridge forms, work done in extending the capture thread's flagelliform fibers contributes substantially to a capture thread's resistance to insect escape (Sahni and Dhinojwala, 2010).

Synergy of flagelliform & glycoprotein and biomechanics of the system

The elastic modulus (stiffness) of each capture thread component and the amount of each material determines their extension during the suspension bridge configuration (Opell et al., 2019; Sahni and Dhinojwala, 2010). This configuration is essential to adhesion, so we predict that the properties of each component have evolved in a synergistic manner to ensure its functionality. Indeed, evidence shows that the suspension

bridge relies on a linkage between these components, with changes in the material properties of either reducing thread adhesion (Guo et al., 2018). We further test the hypothesis of synergy between the suspension bridge components by comparing the elastic modulus and toughness of each component. Additionally, we examine how the amount (volume of glycoprotein and cross-sectional area of flagelliform fibers) are associated. We expect that more extensible droplets are associated with more extensible flagelliform fibers. Additionally, we expect a similar association between toughness and the amount of material in each component. Literature suggests that larger spiders spin larger webs and glue droplets (Sensenig et al., 2010). Therefore, in addition to this association, we also investigate how spider mass is related to the material properties and amounts of each capture thread component. We use phylogenetic generalized least squares to examine these relationships among 14 species of orb weavers and map these thread features onto a phylogeny (Grafen, 1989).

The second objective of this study is to investigate suspension bridge biomechanics and adhesion at different humidities. By characterizing the force on individual droplets as they extend, we are able to use the relationship between length and force to reconstruct the force contributed by droplets across a suspension bridge. Summing these individual droplets gives the inferred adhesive force of the bridge. As orb weavers occupy habitats with different humidity regimes, we predict that low humidity habitat species will generate less adhesion as humidity increases and that high humidity species will increase adhesion with humidity. Our approach also allows us to determine how individual droplet forces are distributed across the suspension bridge. As mentioned earlier, the initial model of outer suspension bridge droplets contributing greater adhesive

force than lesser extended inner droplets has been called into question (Opell and Stellwagen, 2019). Another aspect of bridge formation that has not been fully characterized is the sheet configuration observed at high humidities in some species (Amarpuri et al., 2015b). Instead of distinct droplets, this configuration occurs when droplets merge to form a continuous sheet of glycoprotein, spanning the length of thread contact (Figure 2). It is unclear if adhesion degrades as this configuration is established. Together, these investigations will comprehensively characterize the performance of orb web capture thread adhesion and biomechanics in a broad phylogenetic context.

Materials and methods:

Study species selection

Each of the 14 study species were represented by 10 - 14 mature females collected near Blacksburg, Virginia (Figure 3). Covering two families, our selected orb weavers contain four pairs of congeneric species, allowing us to contrast material properties and biomechanics within genera (Figure 3). These 14 spiders are variable in mass, with *C. turbinata* weighing only 7.2 mg on average compared to *A. aurantia* at an average of 842 mg (Opell and Hendricks, 2009). The capture spiral configuration among these species differs as well, encompassing a broad range of droplet volumes (1369μm^3 – 105,745μm^3) and droplets per millimeter (Table 1). Our local orb weavers forage in various habitats, with some occupying open weedy habitats and others occupying shadier places forests (Bradley, 2013). Other species are nocturnal or adapted to living on human structures (pers. obs.). Broadly, our 14 species can be grouped as either low or high humidity

foragers (Figure 3). Group 1 consists of species that build their webs in exposed habitats and other low humidity environments, while Group 2 consists of species that are nocturnal or high humidity habitat specialists (Figure 3, Table 2).

Web collection

We collected orb web samples shortly after their construction, ensuring fresh threads that were uncontaminated by dust or pollen. Webs were collected early morning, except for the nocturnal species, *L. cornutus* and *N. crucifera*, which were collected around 17:00 hours. A metal frame with double sided tape on its rim was pressed from behind a web, ensuring that a web's native tensions were preserved (3M #9086K29550360). Once adhered, the remaining web was pressed along the outer edge of the frame, isolating the sample. After collecting a web, each site was marked with flagging tape to prevent resampling. Orb weavers were unharmed by this process, fleeing their webs before samples were taken, and were usually found with a new web in the same location the following day. An advantage of this work is its non-destructive nature, with our collecting posing no more of a threat than a rainy day. Once collected, webs were placed in a box to prevent contamination from pollen or further damage. Web samples were taken to the lab within 17 hours of collection, with diurnal samples being brought immediately after collection. We tested droplets and threads at 37%, 55%, and 72% relative humidity (RH) to reflect differences in foraging humidities that these spiders experience in nature.

Thread collection

To prepare individual droplets for testing, we collected a thread on carbon tape covered forceps to ensure natural thread tension was maintained (Cat #77816, Electron Microscope Sciences, Hatfield, PA, USA). These forceps are blocked open to accommodate the width of supports on a microscope slide sampler. After contacting a thread strand with the forceps, we cut the connecting threads with a pair of iris scissors. This sample then spanned the 4.8mm space between the supports of a microscope slide sampler (Opell and Sigler, 2011). We were careful to ensure that these threads were perpendicular to the supports, guaranteeing consistency in the length of the tested thread.

Individual droplet testing

To ensure that only a single droplet contacted our probe, we isolated the central droplet of the suspended strand. Droplets on either side were slid away from the central droplet using a wooden applicator stick that was whittled to a tip. When wetted with distilled water, droplets could easily be moved along the supporting strand. This did not disrupt the aqueous layer of the flagelliform fibers, documented by the formation of small secondary droplets near the central droplet. Once prepared, this slide was placed into a sealed chamber on the mechanical stage of a Mitutoyo FS60 inspection microscope (Mitutoyo America Corp., Aurora, IL, USA). Humidity in the chamber was established using silica desiccant to lower humidity and a distilled water moistened Kimwipe® to increase humidity. A tube attached to a port in the chamber wall allowed us to gently exhale into the chamber to make fine adjustments in humidity.

With the desired humidity achieved, droplets were extended using a probe. Before each test, the 413μm tip of this polished steel probe was cleaned with 100% ethanol on

Whatmann® filter paper. After inserting the probe into a port in the side of the chamber, the probe was locked into a support resting beside the microscope to prevent its movement (Opell et al., 2018b). With the probe locked in, the isolated droplet was brought into contact with the probe tip. To ensure droplet adhesion, the mechanical stage was then advanced an additional 250μm. The movement of the mechanical stage was then reversed by a stepping motor, extending the droplet at a velocity of 69.5 μms^{-1} until the droplet pulled free of the probe. During this time, a video was recorded with a Canon digital Rebel T2i at 60 frames per second.

To determine the glycoprotein volumes within these extended droplets, additional threads from an individual's web were placed across supports of microscope slide samplers and flattened to reveal their glycoprotein cores. A series of three suspended droplets were first photographed at each test humidity and re-photographed after being flattened under a cover slip. Flattening was accomplished using a magnetically triggered device attached to the underside of the chamber's glass cover. We measured the width and length of each suspended droplet (*DW* and *DL*, respectively) using ImageJ 1.50i (https://imagej.nih.gov/ij/). Droplet volume (*DV*) was determined with the following formula.

$$DV = \frac{2\pi \times DW^2 \times DL}{15} \tag{1}$$

From images of flattened droplets, we measured droplet surface area (*DSA*) and glycoprotein surface area (*GSA*). Dividing *DV* by *DSA* yields droplet thickness (*DT*). Multiplying *DT* by *GSA* yields the glycoprotein volume. The mean ratio of glycoprotein

volume to droplet volume at each humidity for an individual was multiplied by the volume of its extended droplets to infer their glycoprotein volume. Two droplets were extended per individual at each humidity.

Glycoprotein material properties

Individual droplet extension videos allowed us to generate true stress-strain curves from which we determined the glycoprotein elastic modulus. The seven steps used to construct these curves rely on properties of the flagelliform fibers and its deflection during extension (Figure 4) (Opell et al., 2018b). In 10 species, flagelliform diameter and elastic modulus values are provided by the literature as measured at approximately 50% RH (Sensenig et al., 2010). Steps 1 and 2 involve measuring the extension of the flagelliform fibers and the resulting force (Figure 4). Steps 3 and 4 involve consolidating the force vectors of each support line onto the extending droplet (Figure 4). Steps 5 and 6 compute true stress as force per cross-sectional area of the glycoprotein, determined by dividing glycoprotein volume by extended droplet length (Figure 4). Step 7 determined true strain using glycoprotein diameter reconfigured as a sphere (Figure 4).

Each stress-strain curve was constructed from measurements of droplet length and support line deflection angle taken at 20% intervals, with 0% extension values measured just prior to droplet extension. Elastic modulus was determined as the linear portion of each curve. Unlike typical stress-strain curves, which begin with a stress of zero, droplets are under tension prior to extension. Consequently, when glycoprotein toughness is computed as the area under the stress-strain curve, we subtract the rectangular area

defined by the stress at the initial of extension and maximum strain from the full area under the curve.

Capture thread material properties and remaining traits

The flagelliform fiber elastic modulus and toughness reported in the literature was measured with a Nano Bionix instrument, covering 10 of our study species (Agilent Technologies, Oak Ridge, TN, USA) (Sensenig et al., 2010). Of the remaining four species lacking this data, two of them (*A. pegnia* and *M. sagitatta*) had their flagelliform fiber diameters measured. Once measured, samples were shipped to the American Museum of Natural History. Here, Dr. Sandra M. Correa-Garwhal determined flagelliform fiber elastic modulus and toughness with a similar Nano Bionix instrument from the literature. We used published flagelliform data from *Cyclosa conica* (Pallas 1772) for *C. turbinata* and *Tetragnatha versicolor* (Walckenaer 1841) for *T. elongata* (Sensenig et al., 2010). Spider mass was taken from the literature (Table 1). Droplets per millimeter was determined by placing our 2mm scale along a capture thread, counting the droplets, and dividing by two.

Evolutionary analyses and software

We used phylogenetic generalized least squares (PGLS) to examine relationships among the capture thread material properties under Brownian Motion, with Pagel's lambda to detect phylogenetic signal (Pagel, 1999). This method accounts for the evolutionary relatedness among species, ensuring that our analysis is not biased by the evolutionary relationships (Felsenstein, 1985; Garamszegi, 2014). The phylogeny used in

this analysis is based on a time calibrated tree produced from BEAST (Dimitrov et al., 2017). *T. elongata* and *C. turbinata* were substituted for their congeners *T. versicolor* and *C. conica*. This tree was then pruned using the phytools R package (R Core Team, 2019; Revell, 2012). Using phytools, we further edited the tree to include sister taxa of four species in our existing phylogeny. These include: *A. pegnia, A. aurantia*, *N. crucifera*, and *M. sagitatta*. Lacking data on the precise divergence of these added species, we placed each of them halfway along the length of its sister's branch. The branch lengths were then set to preserve the ultrametric character of the tree. Lacking a sister taxa or congeneric species, *V. arenata*'s placement was approximated using a different phylogenetic study, which placed it as an outgroup of the genus of *Micrathena* (Garrison et al., 2016). We placed the *V. arenata* branch halfway between *Micrathena* and the rest of the tree, with a branch length that preserved the ultrametric tree.

Having a complete tree, we used PGLS to examine relationships among traits and plot phylomorphospace plots, carried out using the ape, caper, geiger, and phytools packages in R (Orme et al., 2018; Paradis and Schliep, 2019; Pennell et al., 2014; R Core Team, 2019; Revell, 2012). Mesquite was used to trace the evolution of capture thread material properties assuming parsimony(Maddison and Maddison, 2019).

Suspension bridge recording and measurements

Suspension bridges were characterized for six individuals of each species at each humidity (37%, 55%, 72% RH). The suspension bridges were characterized using the same instrumentation and similar procedures employed in single droplet characterization. After placing a thread on a microscope slide sampler and positioning them inside the

humidity-controlled chamber, a 2mm polished steel plate was brought into contact with a thread. This plate was also advanced 250μm to ensure adhesion before a thread was pulled away at 69.5 μms^{-1}. Videos recording this process ended when a thread had completely detached from the plate. In a few cases, support strands snapped, ending the video prematurely. In these cases, we repeated the trial. However, if failure occurred again, then no data was included for that individual at that humidity.

Total suspension bridge adhesion and force distribution

Force-extension length curves, derived from analyses of glycoprotein elastic modulus, allowed us to determine the force on each of a suspension bridge's extended droplets. A linear model explained most regressions of force and droplet length ($P < 0.05$), however a few required other models (Table 2). We measured the lengths of suspension bridge droplets when the central droplet had just begun to extend, ensuring that all droplets contributed adhesive force to the bridge (Figure 1A). Beyond this point, outer droplets begin to detach. A regression formula, specific to each species and humidity, was then used to infer the force of each droplet. These inferred forces of contributing droplets are then summed to obtain the adhesive force of the bridge. The bridge failures, as mentioned in the previous section, were counted as zeros when determining mean adhesion at each humidity.

Inferring adhesion of the sheet configuration

When droplets merge to form a sheet, it is no longer possible to assign a force to each droplet (Figure 2). In these cases, we used the following steps to determine total

sheet force (Figure 5). Just as the sheet begins to pull-off, we can determine its angular deflection with the projected intersection of the flagelliform fibers (Figure 5). Measuring this angle allows us to determine the force on the sheet by incorporating this angle into individual droplet force - angle models. However, this force is partitioned into X- and Y-axis vectors. Opposing, inward-directed X-axis vectors are canceled (F_X). We accounted for this by multiplying F_X by the cosine of angle θ to determine total sheet force perpendicular to the contact plate (F_Y). These new measurements are assimilated into bridge forces values. We used matched pairs to compare the adhesive force of suspension bridges and the sheet configuration.

Statistical software

We used SAS JMP for implementing thread characterization equations (SAS Intitute Inc., Carey, NC).

Results:

Correlations among capture thread features

The values of each species' material property at 55% RH are displayed together (Table 3). A PGLS analysis showed that, of these features, only glycoprotein and flagelliform elastic moduli were related, with glycoprotein elastic modulus being approximately one sixth of the flagelliform fibers elastic modulus (Figure 6A, Table 4). Close relatives tended to cluster together around similar elastic modulus values, despite differing masses (lambda of spider mass < 0.001) (Figure 6B). We found no correlation

between the toughness or volume per millimeter of each thread component (Table 4). High elastic modulus values in one component are often associated with high values in the other component (Figures 6, 7). The toughness between the components lacks this relationship (Figure 8, Table 4). Spider mass was not related to the elastic modulus or toughness of either thread components (Table 4). However, spider mass was correlated with glycoprotein volume per droplet, flagelliform fiber cross-sectional area, and droplets per millimeter (Table 4). The first of these two correlations are positive, with the latter being negative (Figure 9).

Suspension bridge adhesive force across humidity

Suspension bridge adhesive force is characterized at 37, 55, and 72% RH as the sum of each extended droplet (Figure 4). These values also include the inferred adhesive force of the sheet configuration. Our hypothesis predicted that the threads of orb weavers adapted to exposed, low humidity habitats would exhibit greater adhesion at low and intermediate humidity, whereas species found in high humidity habitats and nocturnal species would exhibit greater adhesion at high humidities. To test these predictions, we divided the study species into two broad response groups. Group 1 includes species that exhibit a net decrease in adhesive force as humidity rises and Group 2 species that exhibit the opposite pattern, with increased humidity resulting in greater adhesive force (Figure 10). Of the 14 study species, 11 fit these predictions. As designated by a dashed line, *M. gracilis* was the only high humidity species to be placed with Group 1 species, which were otherwise found in exposed habitats (Figure 10). Two low humidity species, *M. sagittata* and *N. arabesca*, were placed with Group 2 high humidity species. Note that the

lines in each plot are for visualization only and do not represent regression lines. The adhesive force measurements and their standard errors can be found in Table 5.

The distribution of force along a suspension bridge differed among species and sometimes within a species as humidity changed (Table 2). A previous study modeled force across a bridge as decreasing from more extended outer to less extended inner droplets, with the many of the 14 species exhibiting this pattern (Opell and Hendricks, 2009) (Figure 11A, Table 2). However, species found in low humidity habitats showed the opposite pattern at all or most humidities, the only exception being *M. labyrinthea* and *N. arabesca* (Figure 11B, Table 2).

Suspension bridge and sheet force

A two-tailed matched pair analysis revealed few differences in force generated between suspension bridges and sheet configurations. Without dividing up by species or humidity, the average force of each array is similar and not interpreted, as significantly different (Table 6). When separated by humidity, the force generated by each is still comparable, with the 72% RH values being nearly identical (Table 6). Sheet formation only occurs at higher humidities, so we lack sheet measurements at 37% RH.

Discussion:

Synergy between capture thread material properties

Glycoprotein and flagelliform fibers interact to retain insects that strike the web. The adhesive performance of the thread is shaped by its elasticity, with modeling and empirical work revealing a balance of silk elasticity and stickiness that is crucial to

adhesion (Guo et al., 2018; Opell et al., 2018b). Therefore, it is significant that, of the hypothesized associations between glycoprotein and flagelliform fiber features, the only correlated material property was elastic modulus, with glycoprotein elastic modulus being about one-sixth that of flagelliform fiber elastic modulus (Figures 6, 7, Table 4). Maintaining this balance ensures that the structural integrity of the bridge is maintained during adhesion (Guo et al., 2018). A disproportionate increase in glycoprotein elastic modulus would reduce the number of contributing droplets by causing outer droplets to pull off before inner droplet extension was initiated. An uneven stiffening of the flagelliform fibers would reduce their contribution to the work done in pulling a thread from a surface. This work has been shown to make an equally large contribution to insect retention time (Opell et al., 2019; Sahni and Dhinojwala, 2010). Thus, the strong linkage of these elastic moduli may be ensured by selection operating on different capture thread performance criteria.

Glycoprotein toughness was measured in the context of droplet extension to pull-off. However, flagelliform fiber toughness was measured during extension to rupture, something that doesn't occur during thread adhesion (Agnarsson and Blackledge, 2009). Consequently, the reported toughness for flagelliform fibers is much greater than that expressed during normal capture thread function. This probably accounts for our failure to find associations between flagelliform fiber toughness and other thread features (Figure 8, Table 4). However, an association between glycoprotein and flagelliform fiber toughness might have been demonstrated if we had been able to reliably establish the portion of a flagelliform fiber's stress-strain curve that was expressed during suspension bridge formation and, from this, determine the fiber's expressed toughness. These

findings in toughness do not support our hypothesis, but they do suggest that it will be important to characterize the toughness that flagelliform fibers express within the confines of a suspension bridge.

Material invested in capture thread components

Orb weavers differ greatly in mass, over a hundredfold in the case of species included in this study, but spider size and its impact on adhesive performance is not fully understood. Greater spider mass has been linked with higher insect stopping potential, but the effect of mass on the material properties of the capture thread is not explicitly known (Sensenig et al., 2010). Our comparative phylogenetic analyses found no evidence that spider mass is related to the toughness or elastic modulus of either capture thread component (Table 4). The performance of a thread's flagelliform fiber and glycoprotein is determined by a combination of its material properties and the amount of each component.

Flagelliform fiber cross-sectional area and spider mass are positively correlated, a relationship explained by the tendency for larger spiders to spin thicker flagelliform fibers (Figure 9B). Smaller spiders also have a greater number of smaller droplets per millimeter thread length, as shown by a positive correlation of glycoprotein volume with spider mass (Figures 9A, 9C). However, flagelliform fiber cross-sectional area and glycoprotein volume are not correlated and remain unrelated when scaled to flagelliform fiber and glycoprotein volume per millimeter thread length (Table 4). Differences in spiral spacing may be confounding this relationship. More widely spaced capture spirals experience greater individual stress upon prey impact than closely spaced spirals. The

ability of natural selection to strengthen a flagelliform fiber appears to be constrained by two factors: 1. Glycoprotein and flagelliform fiber elastic moduli are highly correlated and 2. Elastic modulus is directly related to toughness. Therefore, this leaves flagelliform fiber diameter as the principal feature upon which selection can act to strengthen a capture thread.

Change in adhesive force varies across humidity and between species

Low and high humidity habitat species groups align well with their bridge forces, showing maximum force at their foraging humidities. These results are consistent with what has been inferred from studies of single droplet measurements (Opell et al., 2013). Although these habitat categories are useful, they suggest that we would observe a continuous increase or decrease in adhesion across the humidity range. While we observe this in most species (11/14), there are some exceptions. For example, *Micrathena sagitatta*, a member of the low humidity group that forages along forest edges, exhibits the greatest adhesion at 55% RH and loses adhesive force at 72% RH. This species was also expected to generate less adhesion as humidity rises, but instead exhibits a net increase in adhesion (Figure 10). *Verrucosa arenata*, a high humidity, deep forest species, demonstrates a similar trend, but exhibits a drop in adhesion at 72% RH, although the force registered at this humidity is much greater than that at 37% RH (Figure 8). Both of these species may be adapted to a broader humidity regime, but this resolution is lost in our characterization of adhesion response to humidity.

Another exception is *N. arabesca*. We characterized this diurnal species as a low humidity species because we find these spiders in the center of webs that are constructed

in low, exposed vegetation, however it has also been reported to forge at night (Bradley, 2013). This contrasts with its congeneric species, *N. crucifera*, which builds its web shortly after dusk and also monitors its web from the hub. *Neoscona crucifera* continues to forage during the following day, but monitors its web from a protected position in surrounding vegetation. Although we have placed these species in different humidity groups, the threads of both exhibit similar force changes across humidities (Figure 10). This may be because each species encounters a wide range of humidity during its long foraging period. The elastic modulus of *N. arabesca* also aligns more closely with that of *N. crucifera* that with that of other low humidity species, being 12 times greater than that of *A. trifasciata*, which places its webs much higher in vegetation and forages only during the day.

The distribution of force along a suspension bridge

An earlier study modeled the distribution of force across a suspension bridge as decreasing from outer droplets to inner droplets (Opell and Hendricks, 2007; Opell and Hendricks, 2009). Although we found this to be the case for most species, seven of the 14 species we examined exhibited the opposite pattern at one humidity or more (Figure 11B, Table 2). This is explained by inter-specific differences in the pattern of force registered by droplets as they extend. In *A. trifasciata*, one of the species that exhibits this pattern at all humidities, a large force is required to initiate droplet extension, after which the thinning glycoprotein filament offers less resistance to elongation and smaller forces are registered (figure 3A, Opell and Stellwagen, 2019). Species that show the opposite pattern are characterized by much less disparity in the forces required to initiate and

extend droplets. Even among species that are characterized by a pattern of increasing force with droplet length, some individuals showed the opposite pattern at some humidities (Table 2).

This pattern of decreasing force with droplet length was only observed in low humidity species. This results in the bridges of these spiders generating more adhesion when their droplets extend only short distances, as would occur during the lower humidity conditions of late morning and afternoon. As humidity increases, droplet extension length would as well, reducing the total force of the bridge. In effect, these species' droplets are "reverse engineered" to accomplish this, avoiding the longer droplet extensions that would reduce their adhesion. The lone low humidity species without this trend, *Neoscona arabesca*, has droplets that generate increasing force as they extend (Table 2). As explained previously, this is consistent with webs that must operate under a broader humidity range.

The impact of merging on adhesion

In some species, a thread's bridge configuration changes as droplets merge to form a sheet under higher humidity. Therefore, merging could be considered as a type failure, along with flagelliform rupture and premature droplet pull-off. Indeed, it would seem that droplet merging would indicate excess water and a deleterious loss of droplet cohesion. While the droplets are indistinct, the thin glycoprotein-aqueous layer sheet appears to accomplish the same biomechanical action as distinct bridge droplets and we were unable to statistically distinguish the forces of the two configurations (Figures 2, 5, Table 6). Thus, instead of signifying failure, sheet formation appears to be a

configurational change. Though more common in some species, this sheet configuration was not always observed. No species exhibited merging in all six trials at a given humidity.

Conclusions:

An orb web's capture thread is a complex and self-assembling natural adhesive that responds to changing environmental conditions (Boutry and Blackledge, 2013; Opell et al., 2018b; Townley and Tillinghast, 2013). The thread's flagelliform fibers and glue droplets play complementary roles in its operation, with the flagelliform fibers supporting and summing each droplet's adhesive force (Opell and Hendricks, 2009). Successful adhesion relies on the hygroscopicity of droplets and the interplay between the thread constituents. We have shown that the elastic modulus of the glycoprotein and flagelliform fibers have evolved synergistically to maintain the integrity of this system (Figures 6, 7). The glycoprotein elastic modulus is typically one-sixth of the flagelliform fibers and, while these properties are correlated, this difference allows for each component to serve its unique role in adhesion. Although spider mass was not related to the material properties of flagelliform fibers or glycoprotein, it did correlate with flagelliform fiber diameter, droplet spacing, and the glycoprotein volume per droplet (Figure 9). Spider mass has been linked to thread functionality previously, and other measurements, such as spiral spacing, may confound the impact of mass on capture thread material properties (Sensenig et al., 2010).

Computing the total adhesive force of the bridge as the sum of its contributing droplets showed that adhesion was usually maximized at the spider's foraging humidity,

consistent with previous modeling and empirical work (Amarpuri et al., 2015b; Opell et al., 2013) (Figure 10). In contrast with an earlier model, which showed a decrease in droplet adhesive force from outer to inner droplets, we found that the bridges of half the species exhibited the opposite pattern (Opell and Hendricks, 2009) (Table 2). Most of these cases involve species with low elastic modulus values. It appears that this results in a larger area of adhesive contact, after which a greater force is necessary to initiate droplet extension. However, after extension begins, the low elastic modulus allows the glycoprotein to extend quickly, reducing the cross-sectional area of the filament, resulting in a substantial drop in force on the filament. Many of these species with "reverse engineered" patterns of droplet adhesion are found in low humidity habitats and have more hygroscopic droplets (Amarpuri et al., 2015b; Jain et al., 2018; Opell et al., 2018a). This pattern of force distribution appears to ensure that a thread's greatest adhesion is expressed soon after contacting a prey (Figure 11B). At high humidity, the suspension bridge may exhibit a sheet configuration as extending droplets merge laterally (Figure 2). At first glance this seems less effective in generating adhesion. However, the sheet configuration generates similar force as the suspension bridge because it accomplishes a similar biomechanical action of bowing the flagelliform fibers (Table 6).

The interplay between the flagelliform fibers and the glycoprotein is a compelling place to examine natural selection. The linkage between these thread components constrains how selection acts because a disproportionate change in one would reduce the functionality of the adhesive (Guo et al., 2018). However, selection must simultaneously maintain the distinct roles of each capture thread component, leading to the synergistic pattern in each component's elastic modulus (Figure 6). At the same time, selection on

the LMMCs composition in the thread's aqueous layer must maintain an appropriate thread hygroscopicity (Jain et al., 2018; Opell et al., 2018b; Townley and Tillinghast, 2013). If future studies were able to measure the "expressed toughness" of the flagelliform fiber during thread adhesion, synergy may be documented by this property as well. The fleeting sheet configuration should be a point of emphasis in future work, as the reason sheets form in some individuals but not others remains unclear. Ultimately, successful adhesion of the capture thread to a prey depends on precise functional integration of many thread components over a very short time span. Orb weaving spiders exhibit many such patterns of integration, which appear to be shaped by a spider's habitat and, to some degree, constrained by its evolutionary history.

Acknowledgments: We would like to acknowledge Dimitar Dimitrov for providing the base phylogeny for this work. SDK would like to acknowledge Marth Muñoz and Josef Uyeda for their feedback on the phylogenetic aspects of this study. We'd also like to thank Nadia Ayoub for providing access to *M. sagitatta* webs and spiders. Dr. Sandra Correa-Garwhal characterized flagelliform fiber material properties that we were unable to in lab and we thank her for her contributions as well.

Chapter 3 Figures

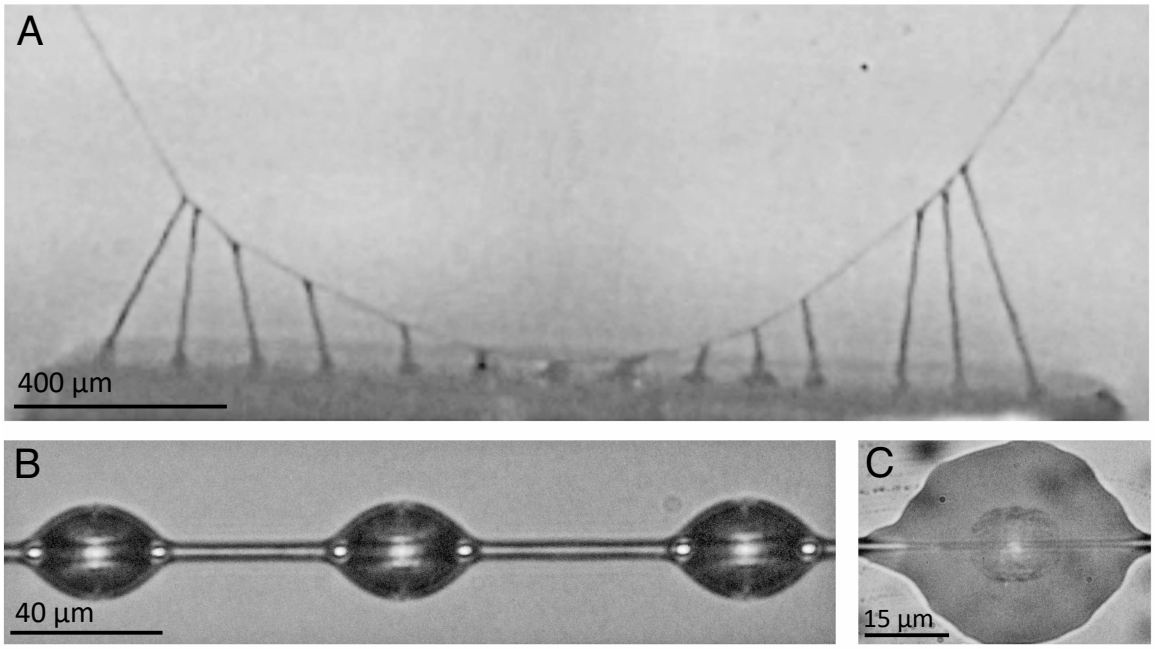

Figure 1: Araneoid capture thread. (A) The suspension bridge configuration, with bowing flagelliform fibers and extending glycoprotein droplets. (B) A view of the capture spiral thread, showing the evenly spaced ellipsoid droplets. (C). Flattened droplet revealing its glycoprotein core.

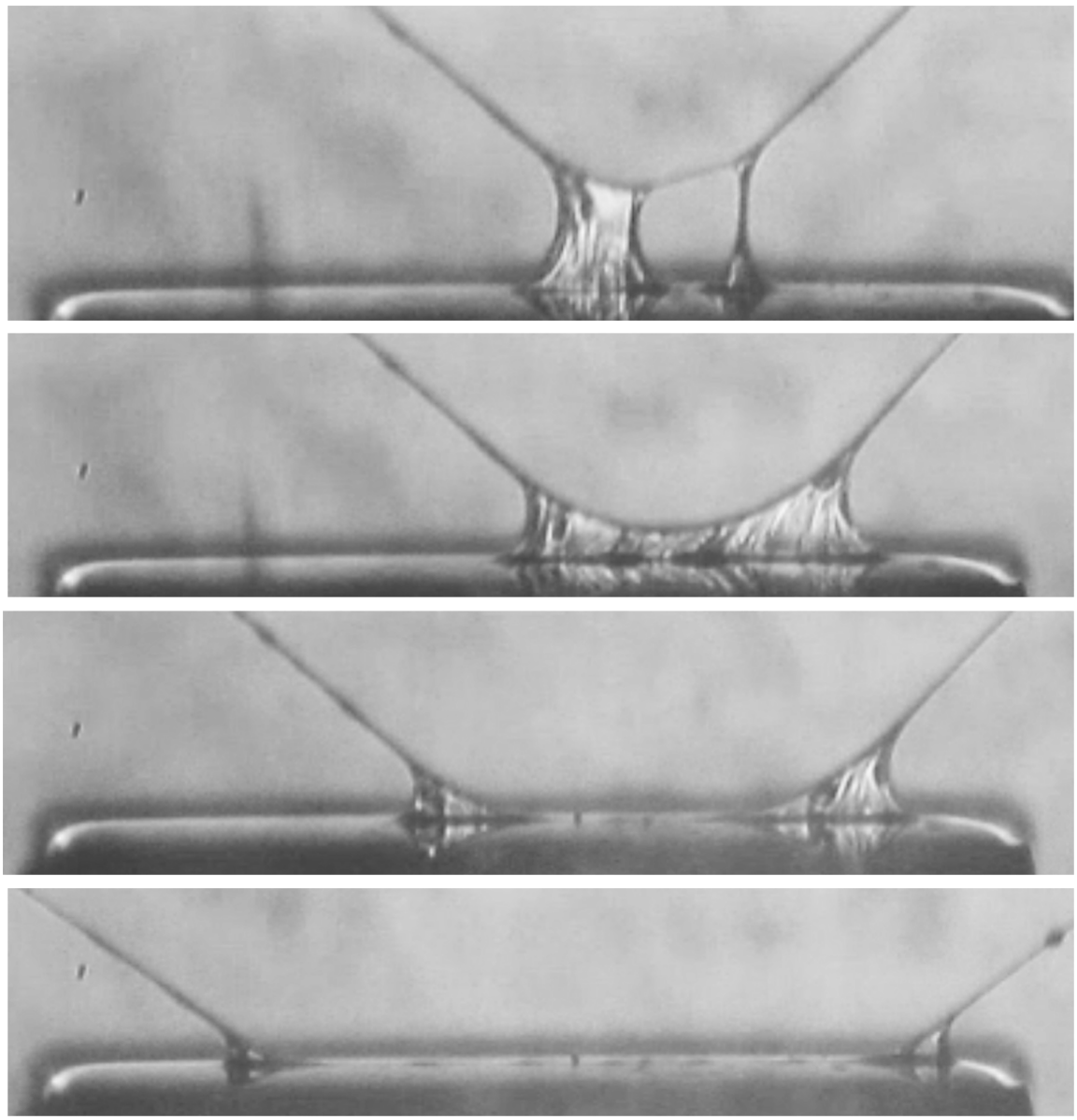

Figure 2: The sheet configuration. As the flagelliform fibers bow, here the droplets merge into a "sheet", a potential consequence of adhesion at high relative humidities. The probe at the bottom of each image is 2μm wide.

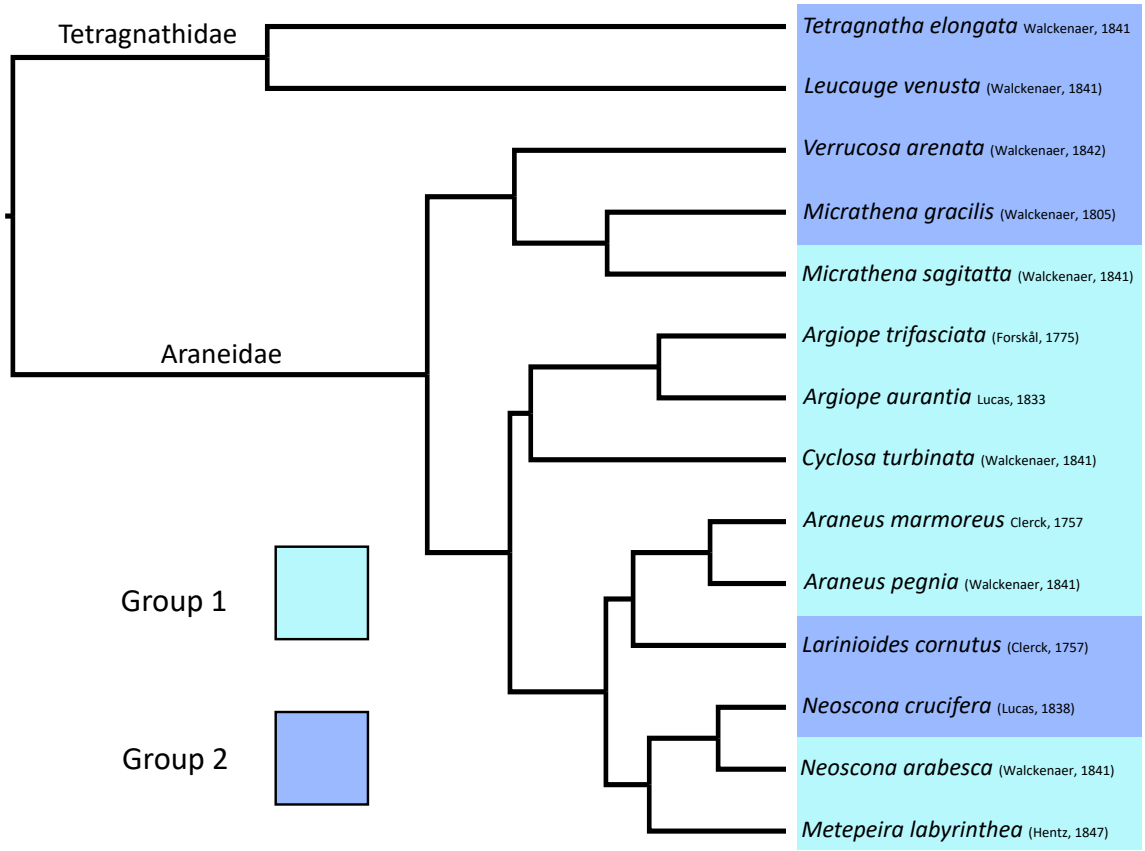

Figure 3: Phylogeny of study species. Topology is based off of phylogeny from Dimitrov et al 2017 and Garrison et al 2016. Group 1 contains low humidity habitat spiders while Group 2 contains high humidity species.

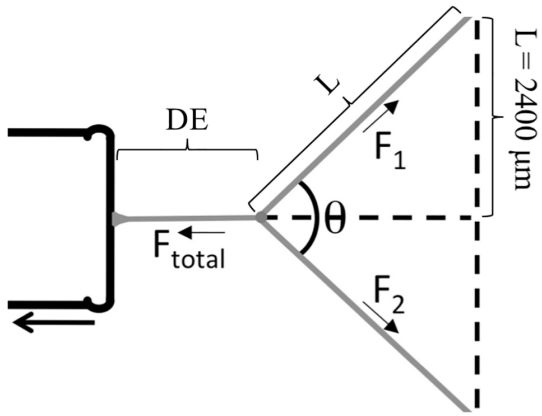

1. $L = 2400\ \mu m \div \sin(\theta/2)$
2. $AE = (L - 2400\ \mu m) \div 2400\ \mu m$
3. $F_1 = F_2 = YM \times \Sigma\ CSA_{AF} \times AE$
4. $F_{total} = 2 \times F_1 \times \sin(90° - (\theta/2))$
5. $CSA_{GF} = GV \div DE$
6. $Stress_T = F_{total} \div CSA_{GF}$
7. $Strain_T = Log_N((DE - DGC) \div DGC)$

AE = extension of axial line
YM = Young's modulus
CSA_{AF} = axial fiber cross sectional area
CSA_{GF} = glycoprotein filament cross sectional area
GV = glycoprotein volume
DGC = diameter of glycoprotein core when configured as a sphere

Each axial fiber (Sensenig et al., 2010)

	Diameter µm	Young's modulus GPa
Argiope aurantia	4.8	0.009
Neoscona crucifera	3.0	0.010
Verrucosa arenata	1.5	0.098

Figure 4: Diagram explaining how the elastic modulus of individual droplets are measured. This figure was originally published as figure 4 of Opell et al 2018b and is cited as such. Used with permission of Brent Opell.

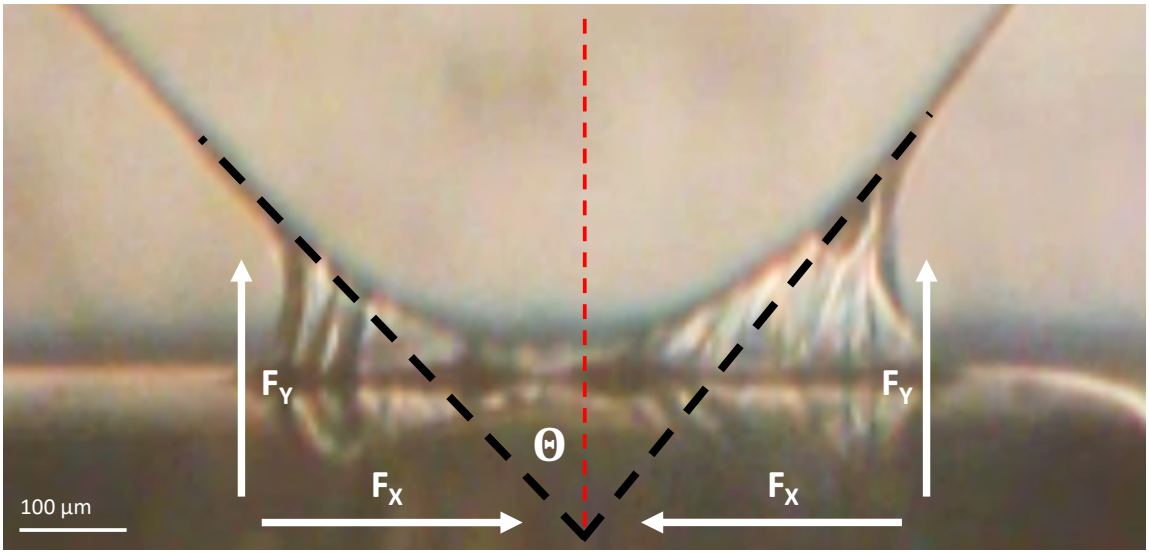

Figure 5: Measuring the angle of the sheet configuration. F_X and F_y denote force vectors in each direction, while theta represents the angle measured and employed in force inference.

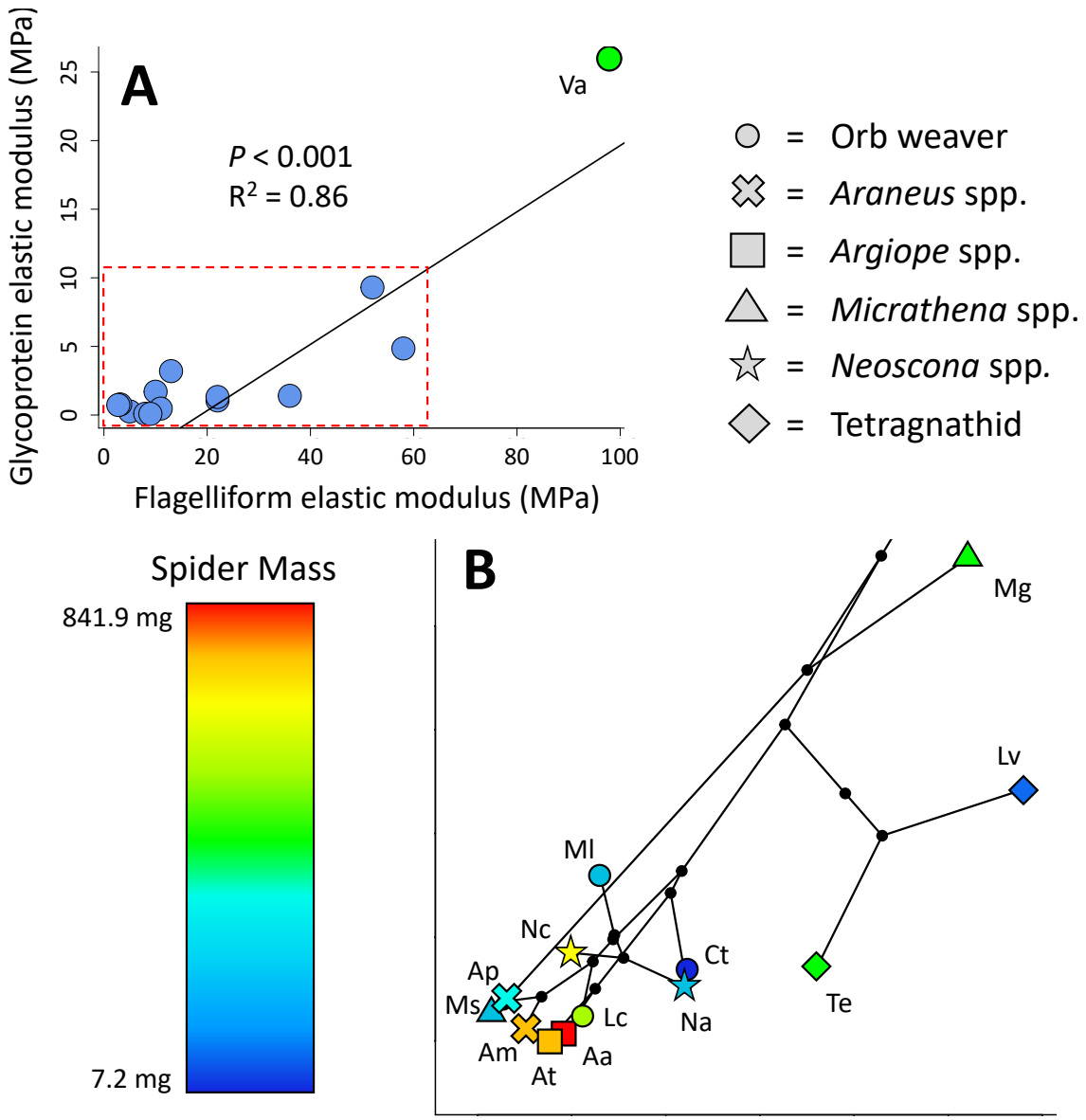

Figure 6: PGLS (A) and phylomorphospace (B) plots showing the relationship between the elastic modulus of each capture thread component. Increased elastic modulus of the flagelliform fibers is associated with increases in the glycoprotein's elastic modulus. Mass is displayed in 6B over the phylomorphospace plot with the identity of each species.

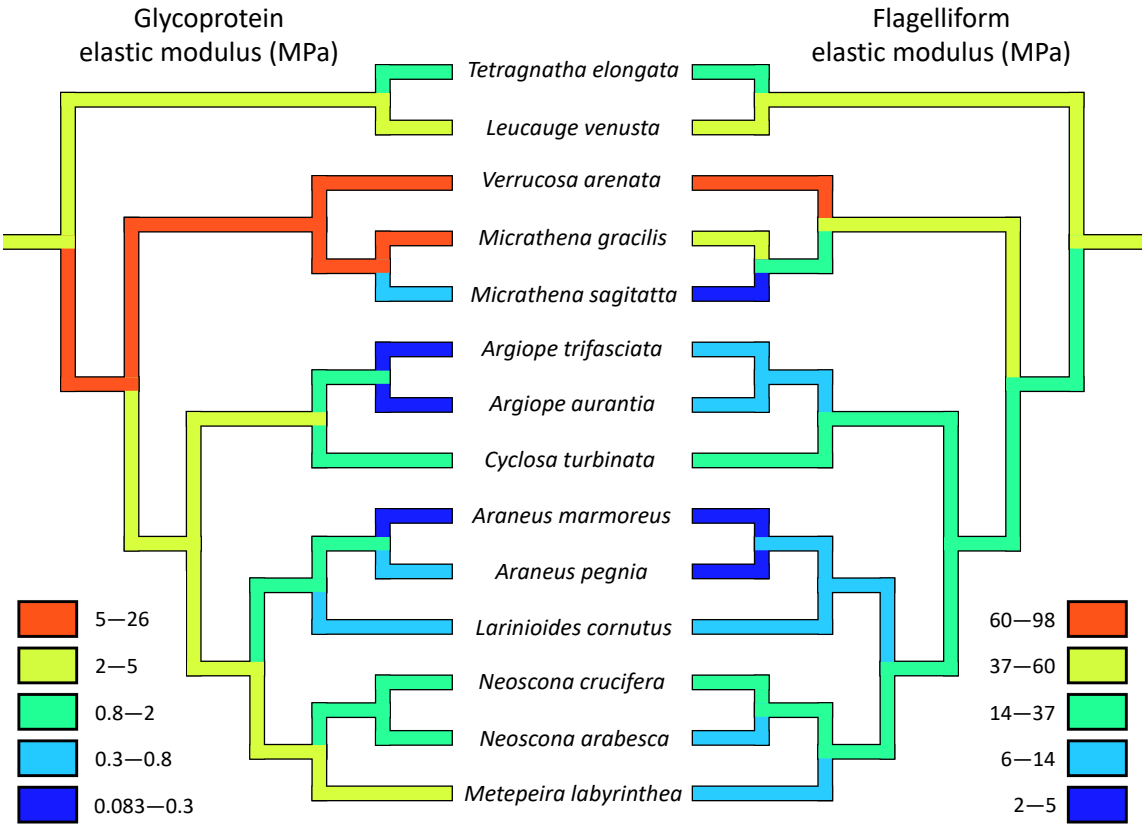

Figure 7: Comparison of the elastic modulus of each capture thread component. As in Figure 6, we see that higher elastic moduli in one component are associated with high values in the other.

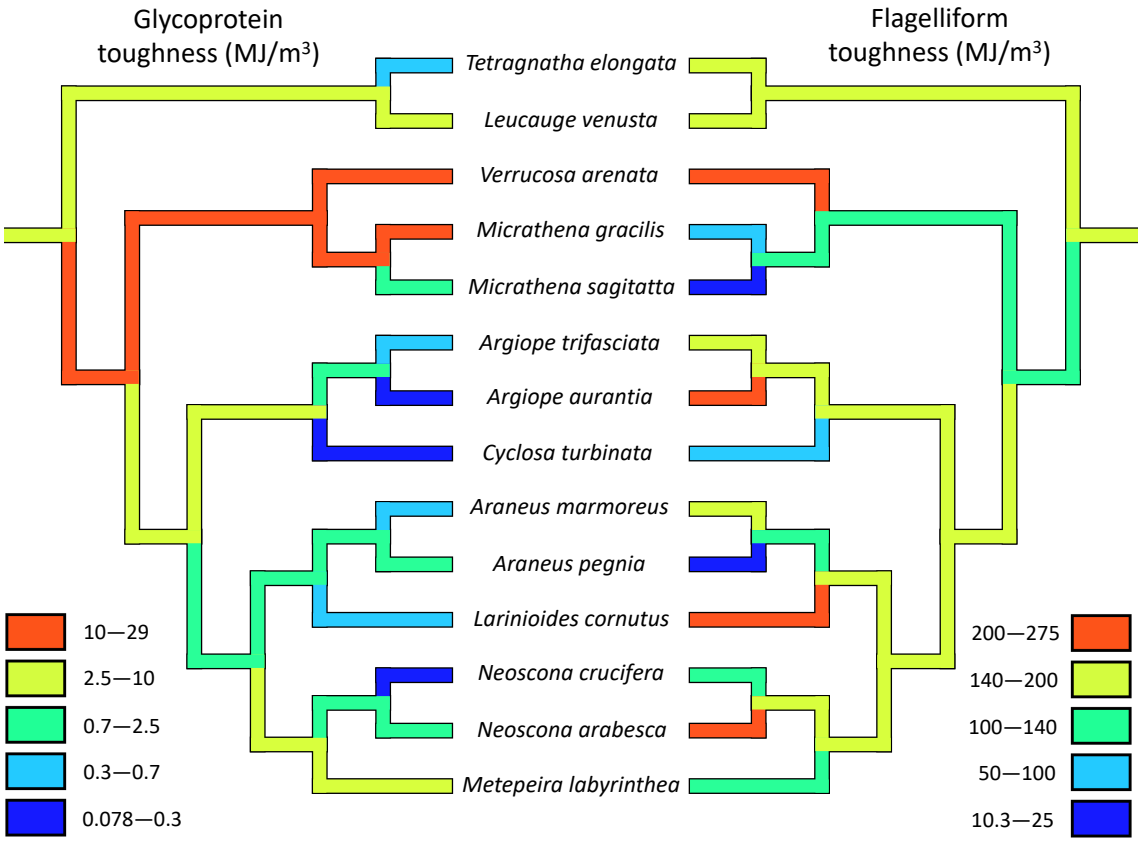

Figure 8: Comparison of the toughness of each capture thread component. While *V. arenata* is an exception, increases in the toughness of one component are not associated with increases in the other.

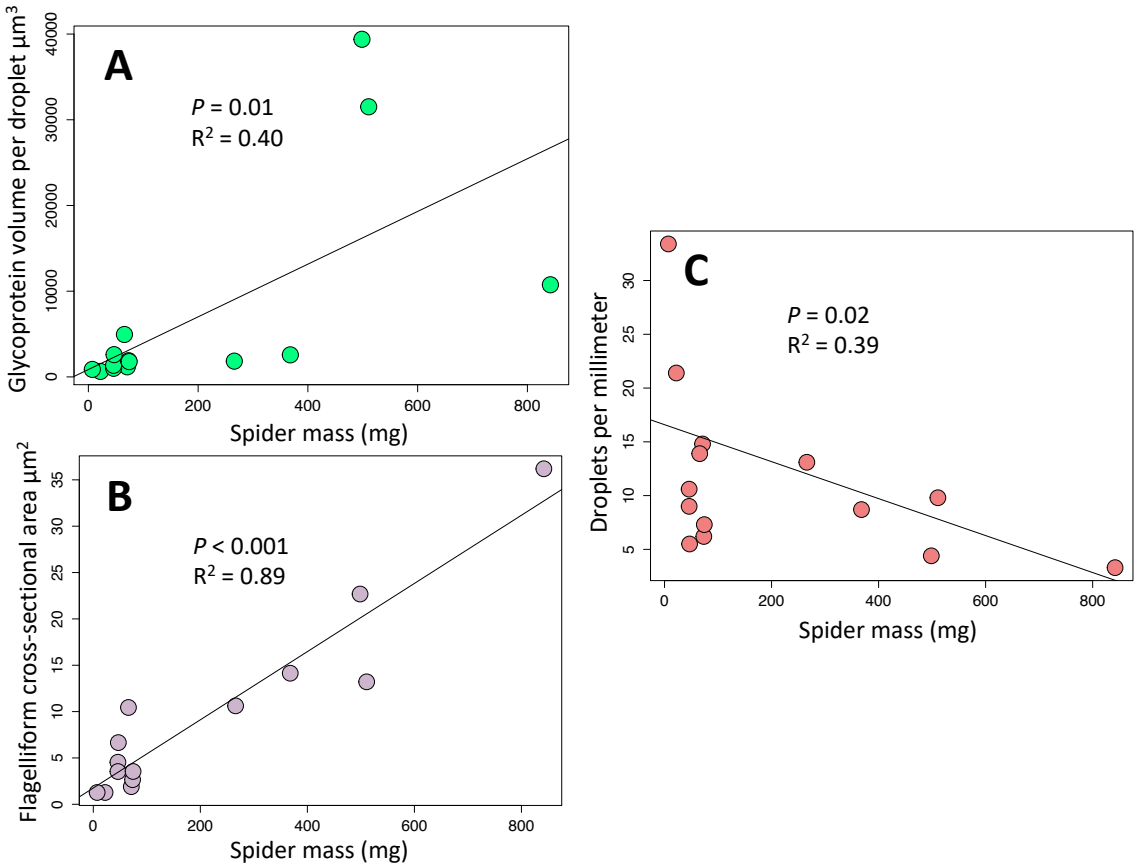

Figure 9: PGLS plots of spider mass against capture thread features. Of our PGLS analyses, these are the only three to produce significant ($P < 0.05$) relationships. From 9A and 9B, higher spider mass is associated with increased glycoprotein volume and flagelliform cross-sectional area. Larger spiders appear to build capture threads with larger and further spaced droplets (9A and 9C).

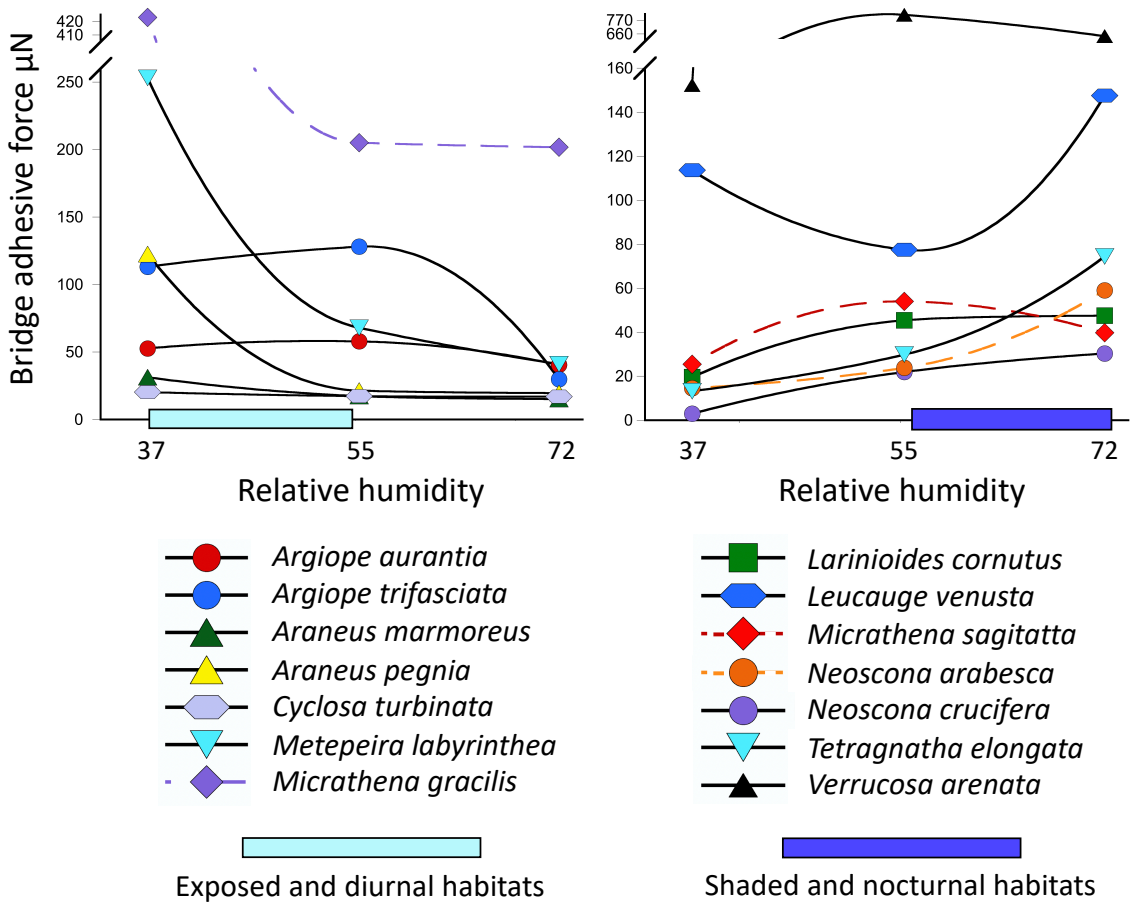

Figure 10: Bridge adhesion force responds in two ways as humidity rises. To the left, species exhibit a net decrease in bridge adhesion with rising humidity. To the right is the opposite, with species generating a net increase in bridge adhesion. Lines are included for visualization and do not represent regressions. Dashed lines represent orb weavers who maximize adhesion outside of their typical foraging humidity, contrary to our prediction of habitat specialization.

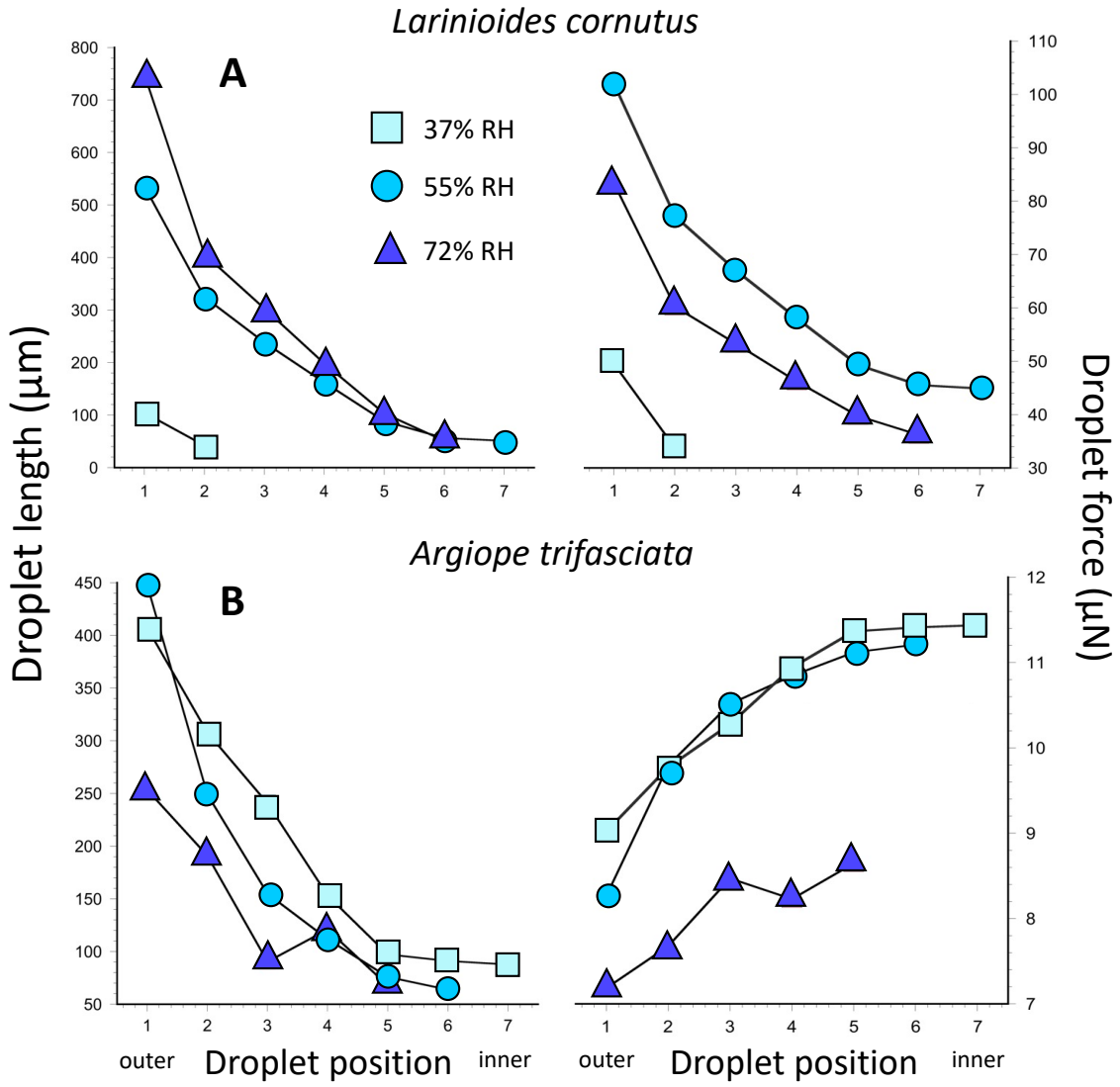

Figure 11: The two patterns of force distribution along a suspension bridge. Both of the plots to the left demonstrate droplet length from the outside of the suspension bridge inward. The two right plots demonstrate droplet force from the outside inward. Figure 11A displays a trend predicted by the literature, droplets on the outside of the bridge contribute the most adhesion. However, half of our species exhibit a trend similar to Figure 11B, with inner droplets generating the most adhesion.

Chapter 3 Tables

Species	Spider mass (mg)	Droplets per mm	Droplet volume μm^3	Glycoprotein volume μm^3	Flagelliform CSA μm^2
Araneus marmoreus	498.5 ± 74.2	4.4 ± 0.8	105745.4 ± 15027.2	39390 ± 14318	**22.7 ± 2.7**
Araneus pegnia	65.7 ± 7.1	13.9 ± 3.1	7059.1 ± 1557.0	4949 ± 1165	10.4 ± 0.2
Argiope aurantia	841.9 ± 138.7	3.3 ± 0.3	86126.2 ± 16474.0	10747 ± 2357	**36.2 ± 3.5**
Argiope trifasciata	510.8 ± 82.0	9.8 ± 1.3	41584.6 ± 6896.5	31512 ± 5622	**13.2 ± 1.3**
Cyclosa turbinata	7.2 ± 0.8	33.4 ± 6.9	2212.2 ± 599.7	873.9 ± 230.7	**1.3 ± 0.02**
Larinioides cornutus	265.9 ± 27.2	13.1 ± 1.8	4789.5 ± 720.2	1837.6 ± 359.4	**10.6 ± 0.9**
Leucauge venusta	22.0 ± 3.1	21.4 ± 2.5	1369.0 ± 213.3	640.4 ± 103.5	**1.3 ± 0.1**
Metepeira labyrinthea	**46 ± 14**	10.6 ± 2.7	3357.1 ± 698.9	1354.9 ± 331.8	**3.5 ± 0.3**
Micrathena gracilis	73.4 ± 9.5	6.2 ± 1.5	7510 ± 1510	1885.9 ± 251.02	**2.7 ± 0.1**
Micrathena sagittata	46.8 ± 5.5	5.5 ± 1.2	8740.0 ± 826.9	2594.5 ± 238.2	6.7 ± 0.2
Neoscona arabesca	**46 ± 24**	9.0 ± 1.0	2506.7 ± 587.5	1004.1 ± 267.8	**4.5 ± 0.4**
Neoscona crucifera	**368 ± 142**	8.7 ± 1.0	13377.6 ± 1715.8	2570.5 ± 685.5	**14.1 ± 2.2**
Tetragnatha elongata	71.0 ± 17.2	14.8 ± 2.2	2700.9 ± 686.4	1176.3 ± 280.2	**1.9 ± 0.3**
Verrucosa arenata	74.3 ± 12.2	7.3 ± 0.5	10281.6 ± 1691.4	1784.9 ± 402.9	**3.5 ± 0.6**

Means ± SD in bold and ± S.E. elsewhere.

Table 1: General spider and thread features. Measurements were taken at 50% – 55% relative humidity. Cross-sectional area is abbreviated to CSA in the last column heading. Data in bold are directly from or derived from Sensenig et al. 2010 and gray data is from Opell & Hendricks 2009. Sample size varies, given the range of sources.

Species	Relationship between droplet force in µN and extension length in µm			Group
	37% RH	55% RH	72% RH	
Araneus marmoreus	**Quadratic***	**Linear**	**Linear**	1
Araneus pegnia	Linear	**Linear**	**Linear**	1
Argiope aurantia	**Quadratic**	**Linear**	**Linear**	1
Argiope trifasciata	**Linear**	**Linear**	**Linear**	1
Cyclosa turbinata	**Quadratic***	**Linear**	**Linear**	1
Metepeira labyrinthea	Linear	Linear	**Linear**	1
Micrathena sagittata	**Linear***	**Linear**	**Linear**	1
Neoscona arabesca	Linear	Linear	Linear	1
Larinioides cornutus	Linear	Linear	Linear	2
Leucauge venusta	Linear	Linear	Linear	2
Micrathena gracilis	Linear*	Linear*	Linear*	2
Neoscona crucifera	Linear	Linear	Linear	2
Tetragnatha elongata	Linear	Linear	Linear	2
Verrucosa arenata	Linear	Linear	Linear	2

* Indicates some values of the force extension curve were excluded, usually at 0% and 100%. Bold values indicate negative relationships.

Table 2: Summary of force-extension length relationships for all species and humidities. We hypothesized that a droplet's contributed force would be related to the droplet's extension length. The best fitting regression models are displayed above, and all relationships were interpreted as significant ($P < 0.05$).

Species	Glycoprotein volume per mm	Flagelliform volume per mm	Glycoprotein elastic modulus MPa	Flagelliform elastic modulus MPa	Glycoprotein toughness MJ/m^3	Flagelliform toughness MJ/m^3
Araneus marmoreus	173316 ± 62999	**22682 ± 2655**	0.26 ± 0.25	**5 ± 2**	0.51 ± 0.32	**163 ± 64**
Araneus pegnia	68791 ± 16194	**10444 ± 234**	0.77 ± 0.22	3.15 ± 0.7	2.05 ± 0.96	10.3 ± 2.6
Argiope aurantia	35465 ± 7778	**36191 ± 3534**	0.08 ± 0.05	**9 ± 11**	0.22 ± 0.09	**211 ± 99**
Argiope trifasciata	308818 ± 55096	**13210 ± 1301**	0.09 ± 0.05	**8 ± 5**	0.63 ± 0.31	**185 ± 65**
*Cyclosa turbinata**	29187 ± 7705	**1272 ± 27**	1.32 ± 0.62	**22 ± 18**	0.12 ± 0.04	**52 ± 28**
Larinioides cornutus	24078 ± 4708	**106189 ± 907**	0.48 ± 0.15	**11 ± 8**	0.55 ± 0.19	**225 ± 84**
Leucauge venusta	13696 ± 2215	**1272 ± 106**	4.85 ± 1.26	**58 ± 46**	7.10 ± 1.17	**148 ± 74**
Metepeira labyrinthea	14363 ± 3517	**3534 ± 277**	3.16 ± 0.85	**13 ± 19**	4.91 ± 1.55	**123 ± 48**
Micrathena gracilis	11693 ± 1556	**2655 ± 141**	9.26 ± 2.49	**52 ± 53**	17.08 ± 2.49	**53 ± 24**
Micrathena sagittata	14273 ± 1310	**6655 ± 225**	0.73 ± 0.25	2.78 ± 0.6	2.10 ± 0.43	23.9 ± 6.9
Neoscona arabesca	9037 ± 2410	**4540 ± 425**	1.06 ± 0.36	**22 ± 13**	0.08 ± 0.03	**133 ± 73**
Neoscona crucifera	22368 ± 5964	**14137 ± 2187**	1.74 ± 0.64	**10 ± 5**	1.49 ± 0.51	**252 ± 99**
*Tetragnatha elongata**	17405 ± 4147	**1901 ± 304**	1.36 ± 0.87	**36 ± 29**	0.58 ± 0.37	**146 ± 94**
Verrucosa arenata	13031 ± 2941	**3534 ± 643**	26.08 ± 7.82	**98 ± 19.9**	28.19 ± 8.86	**272 ± 80**

Means ± SD in bold and S.E. elsewhere.

Table 3: Capture silk material properties. These pairs were analyzed using PGLS (Phylogenetic generalized least squares) to compare the material properties of each capture silk component. Bold features indicate Sensenig et al. 2010 source. Species with * are members of the same genus as their counterpart in Sensenig et al 2010.

Relationship	*P*	R^2
Glycoprotein elastic modulus vs flagelliform elastic modulus (MPa)	< **0.001**	0.86
Glycoprotein toughness vs flagelliform toughness (MJ/m^3)	0.39	0.06
Glycoprotein volume per mm vs flagelliform volume per mm (µm^3/mm)	0.23	0.12
Spider mass (mg) vs.		
glycoprotein elastic modulus (MPa)	0.63	0.02
flagelliform elastic modulus (MPa)	0.41	0.04
glycoprotein toughness (MJ/m^3)	0.59	0.02
flagelliform toughness (MJ/m^3)	0.07	0.25
glycoprotein volume per droplet (µm^3)	**0.01**	0.40
flagelliform fiber cross-sectional area (µm^2)	**< 0.001**	0.89
droplets per millimeter	**0.02**	0.39

Bold values represent significant relationships, interpreted as such when $P < 0.05$.

Table 4: Each PGLS analysis and their results. Each PGLS regression is derived from a comparison of all 14 study species (Figure 3). *P* values in bold represent relationships that are plotted as figures (Figure 6 and 9 respectively).

Species	Suspension bridge force in µN		
	37% RH	55% RH	72% RH
Araneus marmoreus	31.35 ± 3.63	17.37 ± 1.36	3.09 ± 1.98
Araneus pegnia	122.56 ± 25.25	21.45 ± 12.17	19.56 ± 10.71
Argiope aurantia	52.70 ± 5.95	15.28 ± 3.19	10.14 ± 10.14
Argiope trifasciata	113.15 ± 19.09	119.75 ± 25.31	19.00 ± 12.77
Cyclosa turbinata	20.31 ± 3.17	11.82 ± 4.11	1.67 ± 1.67
Larinioides cornutus	19.57 ± 8.91	45.43 ± 9.11	47.55 ± 15.23
Leucauge venusta	113.59 ± 40.71	69.14 ± 25.10	147.53 ± 56.05
Metepeira labyrinthea	253.14 ± 79.62	68.00 ± 17.92	33.19 ± 13.78
Micrathena gracilis	422.86 ± 38.63	95.98 ± 60.99	116.51 ± 59.18
Micrathena sagittata	25.45 ± 4.15	26.95 ± 8.04	13.94 ± 6.15
Neoscona arabesca	14.58 ± 4.25	23.82 ± 3.24	59.04 ± 6.01
Neoscona crucifera	2.98 ± 1.67	21.94 ± 8.69	30.33 ± 12.48
Tetragnatha elongata	13.21 ± 7.38	29.86 ± 12.28	23.50 ± 14.93
Verrucosa arenata	152.33 ± 32.44	815.54 ± 78.85	641.33 ± 40.87

Mean ± standard error.

Table 5: Mean bridge adhesive force for all species and humidities measured.

Species	Bridge force µN	Sheet force µN	*P*
All species and humidities	73.23	61.75	0.5271
55% Relative humidity	104.62	78.64	0.4765
72% Relative humidity	48.82	48.61	0.9911

Table 6: Matched pairs between bridge and sheet configurations. *P* values represent results from a two-tailed t-test.

References

Agnarsson, I. and Blackledge, T. A. (2009). Can a spider web be too sticky? Tensile mechanics constrains the evolution of capture spiral stickiness in orb-weaving spiders. *J. Zool.* **278**, 134–140.

Amarpuri, G., Chaurasia, V., Jain, D., Blackledge, T. A. and Dhinojwala, A. (2015a). Ubiquitous distribution of salts and proteins in spider glue enhances spider silk adhesion. *Sci. Rep.* **5**,.

Amarpuri, G., Zhang, C., Diaz, C., Opell, B. D., Blackledge, T. A. and Dhinojwala, A. (2015b). Spiders Tune Glue Viscosity to Maximize Adhesion. *Am. Chem. Soc.* **9**, 11472–11478.

Blackledge, T. A. and Hayashi, C. Y. (2006). Silken toolkits: biomechanics of silk fibers spun by the orb web spider Argiope argentata (Fabricius 1775). *J. Exp. Biol.* **209**, 2452–2461.

Blackledge, T. A., Kuntner, M. and Agnarsson, I. (2011). *The form and function of spider orb webs. Evolution from silk to ecosystems.*

Boutry, C. and Blackledge, T. A. (2013). Wet webs work better: Humidity, supercontraction and the performance of spider orb webs. *J. Exp. Biol.* **216**, 3606–3610.

Bradley, R. A. (2013). *Common Spiders of North America.* Berkeley, CA: University of Califronia Press.

Coddington, J. A. (1989). Spinneret Silk Spigot Morphology: Evidence for the Monophyly of Orbweaving Spiders, Cyrtophorinae (Araneidae), and Group Theridiidae plus Nesticidae. *J. Arachnol.* **17**, 71–95.

Corrales-Urena, Y. R., Sanchez, A., Pereira, R., Rischka, K., Kowalik, T. and Vega-Baudrit, J. (2017). Extracellular micro and nanostructures forming the velvet worm solidified adhesive secretion. *Mater. Res. Express* **4**,.

DeMoor, S., Herbert Waite, J., Jangoux, M. and Flammang, P. (2003). Characterization of the adhesive from Cuvierian tubules of the sea cucumber Holothuria forskali (Echinodermata, Holothuroidea). *Mar. Biotechnol.* **5**, 45–57.

Dickinson, G. H., Vega, I. E., Wahl, K. J., Orihuela, B., Beyley, V., Rodriguez, E. N., Everett, R. K., Bonaventura, J. and Rittschof, D. (2009). Barnacle cement: a polymerization model based on evolutionary concepts. *J. Exp. Biol.* **212**, 3499–3510.

Dimitrov, D., Benavides, L. R., Arnedo, M. A., Giribet, G., Griswold, C. E., Scharff, N. and Hormiga, G. (2017). Rounding up the usual suspects: a standard target-gene approachfor resolving the interfamilial phylogenetic relationships ofecribellate orb-weaving spiders with a new family-rank classification(Araneae, Araneoidea). *Cladistics* **33**, 221–250.

Edmonds, D. T. and Vollrath, F. (1992). The Contribution of Atmospheric Water Vapour to the Formation and Efficiency of a Spider's Capture Web. *R. Soc.* **248**, 145–148.

Elettro, H., Neukirch, S., Vollrath, F. and Antkowiak, A. (2016). In-drop capillary spooling of spider capture thread inspires hybrid fibers with mixed solid–liquid mechanical properties. *PNAS* **113**, 6143–6147.

Felsenstein, J. (1985). Phylogenies and the comparative method. *Am. Nat.* **125**, 1–15.

Foelix, R. F. (2011). *Biology of Spiders.* 3rd ed. New York, NY: Oxford Univeristy Press.

Garamszegi, L. Z. (2014). *Modern phylogenetic comparative methods and their application in evolutionary biology.*

Garrison, N. L., Rodriguez, J., Agnarsson, I., Coddington, J. A., Griswold, C. E., Hamilton, C. A., Hedin, M., Kocot, K. M., Ledford, J. M. and Bond, J. E. (2016). Spider

phylogenomics: untangling the Spider Tree of Life. *PeerJ* **4**, 1719–1754.
Grafen, A. (1989). The phylogenetic regression. *Philosophical Transactions of The Royal Society of London*. **326**, 119-157.
Guo, Y., Chang, Z., Guo, H. Y., Fang, W., Li, Q., Zhao, H. P., Feng, X. Q. and Gao, H. (2018). Synergistic adhesion mechanisms of spider capture silk. *J. R. Soc. Interface* **15**,.
Guo, Y., Zhao, H.-P., Feng, X.-Q. and Gao, H. (2019). On the robustness of spider capture silk's adhesion. *Extrem. Mech. Lett.* **29**,.
Huang, Y., Wang, Y., Sun, L., Agrawal, R. and Zhang, M. (2015). Sundew adhesive: a naturally occurring hydrogel. *J. R. Soc. Interface* **12**,.
Jain, D., Amarpuri, G., Fitch, J., Blackledge, T. A. and Dhinojwala, A. (2018). Role of Hygroscopic Low Molecular Mass Compounds in Humidity Responsive Adhesion of Spider's Capture Silk. *Biomacromolecules* **19**, 3048–3057.
Kelly, S. P., Sensenig, A. T., Lorentza, K. A. and Blackledge, T. A. (2011). Damping capacity is evolutionarily conserved in the radial silk of orb-weaving spiders. *Zoology* **114**, 233–238.
Krausko, M., Perutka, Z., Šebela, M., Šamajová, O., Šamaj, J., Novák, O. and Pavlovič, A. (2017). The role of electrical and jasmonate signalling in the recognition of captured prey in the carnivorous sundew plant Drosera capensis. *New Phytol.* **213**, 1818–1835.
Maddison, W. P. and Maddison, D. R. (2019). Mesquite: a modular system for evolutionary analysis.
Mead-Hunter, R., King, A. J. C. and Mullins, B. J. (2012). Plateau Rayleigh instability simulation. *Langmuir* **28**, 6731–6735.
Olivencia, A. O., Claver, J. P. C. and Alcatraz, J. A. D. (1995). Floral and reproductive biology of Drosophyllum lusitanicum (L.) Link (Droseraceae). *Bot. J. Linn. Soc.* **118**, 331–351.
Opell, B. D. and Hendricks, M. L. (2007). Adhesive recruitment by the viscous capture threads of araneoid orb-weaving spiders. *J. Exp. Biol.* **210**, 553–560.
Opell, B. D. and Hendricks, M. L. (2009). The adhesive delivery system of viscous capture threads spun by orb-weaving spiders. *J. Exp. Biol.* **212**, 3026–3034.
Opell, B. D. and Sigler, S. E. K. M. A. (2011). Humidity affects the extensibility of an orb-weaving spider's viscous thread droplets. *J. Exp. Biol.* **214**, 2988–2993.
Opell, B. D. and Stellwagen, S. D. (2019). Properties of orb weaving spider glycoprotein glue change during Argiope trifasciata web construction. *Sci. Rep.* **9**, 1–11.
Opell, B. D., Markley, B. J., Hannum, C. D. and Hendricks, M. L. (2008). The contribution of axial fiber extensibility to the adhesion of viscous capture threads spun by orb-weaving spiders. *J. Exp. Biol.* **211**, 2243–2251.
Opell, B. D., Karinshak, S. E. and Sigler, M. A. (2013). Environmental response and adaptation of glycoprotein glue within the droplets of viscous prey capture threads from araneoid spider orb-webs. *J. Exp. Biol.* **216**, 3023–3034.
Opell, B. D., Andrews, S. F., Karinshak, S. E. and Sigler, M. A. (2015). The stability of hygroscopic compounds in orb-web spider viscous thread. *J. Arachnol.* **43**, 152–157.
Opell, B. D., Buccella, K. E., Godwin, M. K., Rivas, M. X. and Hendricks, M. L. (2017). Humidity-mediated changes in an orb spider's glycoprotein adhesive impact prey retention time. *J. Exp. Biol.* **220**, 1313–1321.
Opell, B. D., Jain, D., Dhinojwala, A. and Blackledge, T. A. (2018a). Tuning orb spider glycoprotein glue performance to habitat humidity. *J. Exp. Biol.* **221**,.
Opell, B. D., Clouse, M. E. and Andrews, S. F. (2018b). Elastic modulus and toughness of orb

spider glycoprotein glue. *PLoS One* **13**,.
Opell, B. D., Burba, C. M., Deva, P. D., Kin, M. H. Y., Rivas, M. X., Elmore, H. M. and Hendricks, M. L. (2019). Linking properties of an orb-weaving spider's capture thread glycoprotein adhesive and flagelliform fiber components to prey retention time. *Ecol. Evol.* 1–14.
Orme, D., Freckleton, R., Thomas, G., Petzoldt, T., Fritz, S. A., Isaac, N. and Pearse, W. (2018). caper: Comparative Analyses of Phylogenetics and Evolution in R.
Pagel, M. (1999). Inferring historical patterns of biological evolution. *Nature*. **401**, 877-884.
Paradis, E. and Schliep, K. (2019). ape 5.0: an environment for modern phylogenetics and evolutionary analyses in R. *Bioinformatics* **35**, 526–528.
Pennell, M. W., Eastman, J. M., Slater, G. J., Brown, J. W., Uyeda, J. C., Fitzjohn, R. G., Alfaro, M. E. and Harmon, L. J. (2014). Geiger v2.0: An expanded suite of methods for fitting macroevolutionary models to phylogenetic trees. *Bioinformatics* **30**, 2216–2218.
R Core Team (2019). R: A language and environment for statistical computing.
Revell, L. J. (2012). phytools: an R package for phylogenetic comparative biology (and other things). *Methods Ecol. Evol.* **3**, 217–223.
Russell, A. P., Stark, A. Y. and Higham, T. E. (2019). The Integrative Biology of Gecko Adhesion: Historical Review, Current Understanding, and Grand Challenges. *Integr. Comp. Biol.* **59**, 101–116.
Sahni, V. and Dhinojwala, A. (2010). Viscoelastic solids explain spider web stickiness. *Nat. Commun.* **1**, 1–4.
Sahni, V., Miyoshi, T., Chen, K., Jain, D., Blamires, S. J., Blackledge, T. A. and Dhinojwala, A. (2014). Direct Solvation of Glycoproteins by Salts in Spider Silk Glues Enhances Adhesion and Helps To Explain the Evolution of Modern Spider Orb Webs. *Biomacromolecules* **15**, 1225–1232.
Santos, R. and Flammang, P. (2012). Is the adhesive material secreted by sea urchin tube feet species-specific? *J. Morphol.* **273**, 40–48.
Santos, R., da Costa, G., Franco, C., Gomes-Alves, P., Flammang, P. and Coelho, A. V. (2009). First insights into the biochemistry of tube foot adhesive from the sea urchin Paracentrotus lividus (Echinoidea, Echinodermata). *Mar. Biotechnol.* **11**, 686–698.
SAS Intitute Inc. NC, C. JMP Pro, 13.
Sensenig, A. T., Agnarsson, I. and Blackledge, T. A. (2010). Behavioral and biomaterial coevolution in spider orb webs. *J. Evol. Biol.* **23**, 1839–1856.
Sensenig, A. T., Lorentz, K. A. and Kelly, S. P. (2012). Spider orb webs rely on radial threads to absorb prey kinetic energy. *J. R. Soc. Interface* **9**, 1880–1892.
Stark, A. Y., Davis, H. R. and Harrison, W. K. (2019). Shear adhesive performance of leaf-cutting ant workers (Atta cephalotes). *Biotropica* **51**, 572–580.
Swanson, B. O., Blackledge, T. A., Summers, A. P. and Hayashi, C. Y. (2006). Spider dragline silk: correlated and mosaic evolution in high-performance biological materials. *Evolution (N. Y)*. **60**, 2539–2551.
Tillinghast, E. K., Townley, M. A., Wight, T. N., Uhlenbruck, G. and Janssen, E. (1993). The adhesive glycoprotein of the orb of Argiope aurantia (Araneae, Araneidae). *Mater. Res. Soc. Symp. Proc.* **259**, 154–165.
Townley, M. A. and Tillinghast, E. K. (2013). *Aggregate Silk Gland Secretions of Araneoid Spiders*. (ed. Nentwig, W.) Springer-Verlag Berlin Heidelberg.
Townley, M. A., Bernstein, D. T., Gallagher, K. S. and Tillinghast, E. K. (1991).

Comparative study of orb web hygroscopicity and adhesive spiral composition in three araneid spiders. *J. Exp. Zool.* **259**, 154–165.

Vollrath, F. (2000). Strength and structure of spiders' silks. *Rev. Mol. Biotechnol.* **74**, 67–83.

Vollrath, F. and Tillinghast, E. K. (1991). Glycoprotein glue beneath a spider web's aqueous coat. *Naturwissenschaften* **78**, 557–559.

Waite, H. J. (2017). Mussel adhesion - essential footwork. *J. Exp. Biol.* **220**, 517–530.

Wang, C. S., Ashton, N. N., Weiss, R. B. and Stewart, R. J. (2014). Peroxinectin catalyzed dityrosine crosslinking in the adhesive underwater silk of a casemaker caddisfly larvae, Hysperophylax occidentalis. *Insect Biochem. Mol. Biol.* **54**, 69–79.

Wolff, J. O. and Gorb, S. N. (2016). *Attachment Structures and Adhesive Secretions in Arachnids*. New York, NY: Springer.

Wolff, J. O., Grawe, I., Wirth, M., Karstedt, A. and Gorba, S. N. (2015). Spider's super-glue: thread anchors are composite adhesives with synergistic hierarchical organization. *Soft Matter* **11**, 2394–2403.

Wolff, J. O., Paterno, G. B., Liprandi, D., Ramírez, M. J., Bosia, F., Marie E. HerbersteinMeijden, A. van der, Michalik, P., Smith, H. M., Jones, B. R., Ravelo, A. M., et al. (2019). Evolution of aerial spider webs coincided with repeated structural optimization of silk anchorages. *Evolution (N. Y).* **x**, 1–13.

Zhao, Q., Lee, D. W., Ahn, B. K., Seo, S., Kaufman, Y., Israelachvili, J. N. and Waite, J. H. (2016). Underwater contact adhesion and microarchitecture in polyelectrolyte complexes actuated by solvent exchange. *Nat. Mater.* **15**, 407–412.

Chapter 4: Conclusion

Araneoid orb weavers produce a capture spiral thread with viscoelastic glue droplets (Sahni and Dhinojwala, 2010). Their glycoprotein core gives them the ability to adhere and extend as insects strike the orb web and struggle to escape (Townley and Tillinghast, 2013). The LMMCs in the layer surrounding this glycoprotein confer hygroscopicity, causing droplet to volume track changes in relative humidity (Amarpuri et al., 2015). Species have adapted to habitats with different humidity regimes by altering this LMMC composition (Opell et al., 2013). This study documents that individual droplets are able to repeatedly adhere, extend, and pull-off of a surface. For orb weavers, this "cycling" behavior means that droplets are reusable during a prey capture bout because detached droplets can re-adhere during the struggle. From a material science perspective, the ability to cycle, combined with droplet response to relative humidity, qualifies orb weaver droplets as smart materials for the first time. Future research that attempts to mimic these glue droplets should take droplet cycling into account because their reusability increases their already "green" potential, along with their ability to self-organize.

Insect capture is not the function of single droplets. Instead, it is the result of the integrated contributions from the flagelliform fibers and multiple droplets. This integration takes the form of a suspension bridge configuration, whose bowing flagelliform fibers sum the adhesion of each contributing droplet (Opell and Hendricks, 2009). The remainder of this study sought to characterize the evolution of the material properties of this system, as well as the biomechanics at play during adhesion. Knowing the complementary roles that the flagelliform fibers and glycoprotein play during adhesion, we predicted that the evolution of their material properties would reflect this relationship. However, PGLS analyses of 14 orb weaving species supported this "synergy hypothesis" only for the elastic moduli of each capture thread

component, with toughness lacking a relationship. The elastic modulus of the flagelliform fibers is typically six times that of the glycoprotein. This is consistent with the role that each play in the suspension bridge, with the stiffer flagelliform fibers supporting the highly extensible glycoprotein core within each droplet. This synergy between the two components has evolved to preserve the integrity of the suspension bridge during insect capture. If the elasticity of one component deviates, this mismatch compromises adhesion by minimizing the contribution of the other (Guo et al., 2018). Using PGLS analyses, we also examined the impact of spider mass on the material properties of the capture thread, as mass has been linked to orb web material performance. However, we were unable to demonstrate a relationship between spider mass and the material properties of either flagelliform fibers or glycoprotein.

To further characterize the biomechanics of the suspension bridge, we computed suspension bridge adhesion as the sum of each of its contributing droplets. We did this at 37%, 55%, and 72% relative humidities, allowing us to determine how adhesion changed with humidity, and test the hypothesis that adhesive performance has been tuned to a species' foraging humidity. The 14 study species were assigned to low and high humidity groups, which, we predicted, would generate the most adhesion at 37% and 72% relative humidity, respectively. Largely, this was true, with only three species' threads generating more adhesion outside their typical foraging humidity. While this is strong evidence that capture thread performance is adapted to the humidity of its spider, some orb weavers appear to spin thread that functions over a broader humidity range than others.

Our system of measuring each droplet's contribution allowed us to characterize the distribution of force along a suspension bridge. The initial modeling of the system predicted that outer droplets contribute the most adhesive force. While we find evidence for this in seven

species, the remaining orb weavers demonstrate the opposite pattern, with interior droplets generating the most adhesion. Most of these cases involve species with low elastic modulus values. It appears that this results in a larger area of adhesive contact, after which a greater force is necessary to initiate droplet extension. However, after extension begins, the low elastic modulus allows the glycoprotein to extend quickly, reducing the cross-sectional area of the filament and resulting in a substantial drop in force on the filament. Many of these species with "reverse engineered" patterns of droplet adhesion are found in low humidity habitats and have more hygroscopic droplets (Amarpuri et al., 2015; Jain et al., 2018; Opell et al., 2018a). This pattern of force distribution appears to ensure that a thread's greatest adhesion is expressed soon after contacting a prey.

At high humidity, the suspension bridge may exhibit a sheet configuration as extending droplets merge laterally. At first glance this seems less effective in generating adhesion. However, the sheet configuration generates similar force as the suspension bridge. This is explained by the fact that, as in a typical suspension bridge, the sheet configuration accomplishes a similar biomechanical action of dispersed glycoprotein adhesive serving to bow the flagelliform fibers.

The interplay between the flagelliform fibers and the glycoprotein is a compelling place to examine natural selection. The linkage between these thread components constrains how selection acts because a disproportionate change in one would reduce the functionality of the adhesive system (Guo et al., 2018). However, selection must simultaneously maintain the distinct roles of each capture thread component, leading to the synergistic pattern in each component's elastic modulus. At the same time, selection on the LMMCs composition in the thread's aqueous layer must maintain a thread hygroscopicity necessary to ensure appropriate glycoprotein

viscosity (Amarpuri et al., 2015; Opell et al., 2018b; Townley and Tillinghast, 2013). Currently, one of the biggest challenges to more fully understanding this system is the lack of data on the "expressed toughness" of the flagelliform fiber during normal thread adhesion. If these data were available, it is possible that synergy could be documented in this property as well. The fleeting sheet configuration should also be a point of emphasis in future work, as the reason sheets form in some individuals of a species but not others remains unclear. Ultimately, successful adhesion of the capture thread to a prey depends on precise functional integration of many thread components over a very short time span. Orb weaving spiders exhibit many such patterns of integration, which appear to be shaped by a spider's habitat and, to some degree, constrained by its evolutionary history.

References

Amarpuri, G., Zhang, C., Diaz, C., Opell, B. D., Blackledge, T. A. and Dhinojwala, A. (2015). Spiders Tune Glue Viscosity to Maximize Adhesion. *Am. Chem. Soc.* **9**, 11472–11478.

Guo, Y., Chang, Z., Guo, H. Y., Fang, W., Li, Q., Zhao, H. P., Feng, X. Q. and Gao, H. (2018). Synergistic adhesion mechanisms of spider capture silk. *J. R. Soc. Interface* **15**,.

Jain, D., Amarpuri, G., Fitch, J., Blackledge, T. A. and Dhinojwala, A. (2018). Role of Hygroscopic Low Molecular Mass Compounds in Humidity Responsive Adhesion of Spider's Capture Silk. *Biomacromolecules* **19**, 3048–3057.

Opell, B. D. and Hendricks, M. L. (2009). The adhesive delivery system of viscous capture threads spun by orb-weaving spiders. *J. Exp. Biol.* **212**, 3026–3034.

Opell, B. D., Karinshak, S. E. and Sigler, M. A. (2013). Environmental response and adaptation of glycoprotein glue within the droplets of viscous prey capture threads from araneoid spider orb-webs. *J. Exp. Biol.* **216**, 3023–3034.

Opell, B. D., Jain, D., Dhinojwala, A. and Blackledge, T. A. (2018a). Tuning orb spider glycoprotein glue performance to habitat humidity. *J. Exp. Biol.* **221**,.

Opell, B. D., Clouse, M. E. and Andrews, S. F. (2018b). Elastic modulus and toughness of orb spider glycoprotein glue. *PLoS One* **13**,.

Sahni, V. and Dhinojwala, A. (2010). Viscoelastic solids explain spider web stickiness. *Nat. Commun.* **1**, 1–4.

Townley, M. A. and Tillinghast, E. K. (2013). *Aggregate Silk Gland Secretions of Araneoid*

Spiders. (ed. Nentwig, W.) Springer-Verlag Berlin Heidelberg.